NASA TECHNICAL NOTE

NASA TN D-2340

HEAT-TRANSFER MEASUREMENTS ON A FLAT PLATE AND ATTACHED FINS AT MACH NUMBERS OF 3.51 AND 4.44

by Earl A. Price, Paul W. Howard, and Robert L. Stallings, Jr.

Langley Research Center
Langley Station, Hampton, Va.

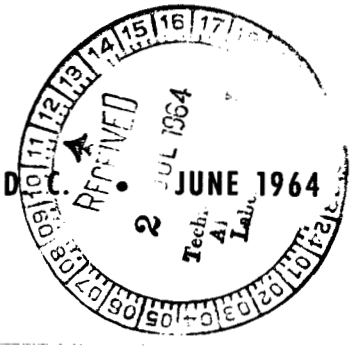

NATIONAL AERONAUTICS AND SPACE ADMINISTRATION • WASHINGTON, D. C. • JUNE 1964

HEAT-TRANSFER MEASUREMENTS ON A FLAT PLATE AND ATTACHED FINS AT MACH NUMBERS OF 3.51 AND 4.44

By Earl A. Price, Paul W. Howard,
and Robert L. Stallings, Jr.

Langley Research Center
Langley Station, Hampton, Va.

NATIONAL AERONAUTICS AND SPACE ADMINISTRATION

For sale by the Office of Technical Services, Department of Commerce,
Washington, D. C. 20230 -- Price $1.00

HEAT-TRANSFER MEASUREMENTS ON A FLAT PLATE AND ATTACHED FINS AT MACH NUMBERS OF 3.51 AND 4.44

By Earl A. Price, Paul W. Howard,
and Robert L. Stallings, Jr.
Langley Research Center

SUMMARY

Heating distributions have been obtained on three fixed-sweep fins (12.87°) of different leading-edge diameters partially submerged in a turbulent boundary layer, as well as on the flat-plate surface adjacent to these fins. Heating rates have also been obtained on a flat plate adjacent to a fin at sweep angles varying from 0° to 69°.

The heating rates obtained on the leading edge of the fins outboard of the sidewall boundary-layer effects are in good agreement with laminar theory. The maximum stagnation-line values obtained in the region subjected to the flow of the turbulent sidewall boundary layer are in good agreement with turbulent theory. The variation of separation distance on the flat plate upstream of the fin leading edge with diameter was found to be approximately linear and relatively independent of boundary-layer thickness. The ratio of the heat-transfer coefficients obtained on the center line of the flat plate with the fins mounted to those obtained on the flat plate alone, h/h_o, upstream of the stagnation line of the fins investigated tends to fall on a single general curve when plotted against the distance from the center line of the fin leading edge in diameters, r/d. In general, $h/h_o \approx 1$ for $r/d > 2.5$ and increases asymptotically, within the span of instrumentation, as the fin leading edge is approached. The correlation of data obtained from a 0.155-inch and a 6-inch boundary layer, using the parameters r/d and h/h_o, indicates that boundary-layer thickness has relatively little, if any, effect on the ratio h/h_o in the interference region.

In general, increasing sweep resulted in a decrease in both the area affected by interference on the flat plate and the magnitude of the heating rates within this interference region. At the high Reynolds number (4.2×10^6), where the boundary layer was turbulent, the maximum measured heating rate nearest the fin, upstream of the fin stagnation line ($r/d = 1.5$), decreases from approximately twice the theoretical turbulent flat-plate value at $\Lambda = 0^{\circ}$ to the undisturbed value at $\Lambda = 40^{\circ}$. Further increases in sweep had only a slight effect on the heating distribution within the entire interference region. At the low Reynolds number (2.5×10^6), the boundary layer remained laminar outside the fin interference region. However, within the interference region the heating rates at the lower sweep angles were of approximately the same magnitude as those obtained at the high Reynolds number, indicating transitional or

turbulent flow. Due to the apparent transitional flow in this region, the effects of sweep are significant on the flat-plate heating rates in the vicinity of the fin throughout the tested range of sweep.

INTRODUCTION

Since the development of vehicles capable of supersonic flight, considerable attention has been focused on the problem of aerodynamic heating in the vicinity of surface protuberances. The absence of suitable theory for predicting heating rates in regions of such disturbed flow has necessitated considerable experimental work for design purposes. References 1 to 6 represent a large portion of the experimental data thus far reported. Included in these references are aerodynamic heating data for both hardware-type models and two- and three-dimensional protuberances of simple shape. The investigations reported in references 1 to 5 were conducted with models mounted on a flat plate, whereas in reference 6 the protuberances were mounted on the cylindrical section of a cone-cylinder model. Each of these investigations included at least one cylindrical protuberance, and references 1, 2, 5, and 6 contain cylindrical protuberances of two different diameters. Data presented in references 1 and 5 for surface heating rates in the vicinity of cylindrical protuberances swept forward 45° and aft 45° indicate that sweep has a strong effect on both the magnitude of adjacent-surface heating and the extent of the separated-flow region. It is the purpose of this investigation to determine the effect of fin leading-edge diameter and sweep on adjacent-surface heating rates and also to obtain a detail heating distribution on three fin-type protuberances partially submerged in a turbulent supersonic boundary layer. Fins of the same geometric size as the three fin-type protuberances have been investigated partially submerged in a hypersonic boundary layer at Mach 8; the results of this investigation are reported in reference 7.

The heat-transfer measurements were made at Mach numbers of 3.51 and 4.44 and at free-stream Reynolds numbers per foot ranging from approximately 2.5×10^6 to 4.2×10^6.

SYMBOLS

b	span of fixed-sweep fins, 18 in. (fig. 4)
c	specific heat of skin material, Btu/lb-°R
d	diameter of fin leading edge, in.
h	heat-transfer coefficient, Btu/ft^2-sec-°R
h_c	experimental heat-transfer coefficient including conduction term, Btu/ft^2-sec-°R

h_L	theoretical stagnation-line heat-transfer coefficient for laminar flow on cylinder of infinite length, Btu/ft^2-sec-$^\circ$R
h_o	experimental heat-transfer coefficient on flat plate alone, Btu/ft^2-sec-$^\circ$R
k	coefficient of thermal conductivity for model skin, Btu/ft-sec-$^\circ$R
l	fin chord length measured from intersection of cylindrical leading edge and fin side panel, in. (fig. 4)
M	free-stream Mach number
n	time limit of integration, sec
r	longitudinal distance on flate plate from axis of symmetry of fin leading edge, in. (fig. 7)
R	free-stream Reynolds number per foot
s	surface distance from stagnation line of fin leading edge, in. (fig. 4)
T	temperature, $^\circ$R
T_e	measured equilibrium temperature of model wall, $^\circ$R
T_w	model wall temperature, $^\circ$R
T_t	stagnation temperature, $^\circ$R
t	time, sec
w	specific weight of skin material, lb/cu ft
x	distance from leading edge of instrumented plate, in. (fig. 1)
x_1, y_1	orthogonal coordinates used in conduction term of equation (5), ft
x_c	longitudinal distance from intersection of cylindrical leading edge and fin side panel, in. (fig. 4)
y	distance from center line of test plate, in. (fig. 1)
z	perpendicular distance from instrumented plate, in. (fig. 4)
δ	boundary-layer thickness, in.
Λ	sweep angle, deg
ϕ	meridian angle, deg (fig. 4)
τ	skin thickness, ft

Subscripts:

m	limit of summation (eq. (4))
s	stagnation line

APPARATUS

Wind Tunnel

The investigation was conducted in the high Mach number test section of the Langley Unitary Plan wind tunnel, which is a continuous-flow, variable-pressure tunnel with a 4- by 4-foot test section. An asymmetric sliding-block nozzle allows variation of the Mach number from 2.3 to 4.65. A detail description of this facility is available in reference 8.

Tunnel Sidewall Instrumented Plate

Each of the fixed-sweep fins investigated was mounted on a 4- by 5-foot instrumented flat plate. The test plate was mounted on the test section access door flush with the tunnel sidewall to utilize the tunnel-sidewall boundary layer. The location of 41 iron-constantan thermocouples on the test surface and the relative location of the three fins tested are illustrated in figure 1. The 0.050-inch stainless-steel skin of the flat plate was insulated from a 0.125-inch-thick filler plate by 0.375-inch-thick hexagonal fiber-glass honeycomb. After the honeycomb was bonded to the test surface and the filler plate, the filler plate was cut into 8- by 8-inch sections. Each of these sections was secured to a steel backing plate by a button that allowed each segment to slide relative to the backing plate. This method of construction was used in order to prevent shearing of the bond due to thermal gradients. A 0.50-inch-diameter plug of the honeycomb was removed at each thermocouple location. A cross section of this sandwich-type construction is shown in figure 2.

Fixed-Sweep-Fin Models

Three fin-type protuberances having a sweep angle of 12.87° with leading-edge diameters of 0.75, 2.00, and 3.50 inches were tested. Each of the models was constructed of 0.040-inch 321 stainless steel and was supported by stiffeners made of a material having low thermal conductivity. Each was instrumented with 39 iron-constantan thermocouples. The locations of the thermocouples are shown in figure 3. The geometric characteristics of the model are presented in figure 4. A photograph of the 3.50-inch-diameter model installed in the test section is presented in figure 5.

Variable-Sweep-Fin Model

The variable-sweep model consisted of a rectangular fin with a 0.25-inch-diameter cylindrical leading edge mounted on a 12- by 21.4-inch support plate. The sweep of the fin was remotely varied through a range from 0° to 69° by a drive system mounted under the plate. The general arrangement of the model and drive system is shown in figure 6. The test surface, a 0.030-inch-thick inconel plate instrumented with 43 iron-constantan thermocouples, was mounted flush with the flat surface of the support plate. A 0.25-inch-wide band of No. 60 carborundum grains was glued to the test plate 1 inch from the leading edge. A minimum air gap of 0.25 inch was maintained between the instrumented plate and the support plate in order to minimize conduction losses. The fin protruded through the slot in the instrumented plate and support plate with a clearance of approximately 0.002 inch on each side. The leading edge of the fin was constantly held in contact with a circular slot in the instrumented plate by means of a high tension spring (see fig. 6). The complete drive system for the fin and the complete lower surface of the instrumented plate were sealed beneath the support plate with a gasket and metal cover. Model dimensions and thermocouple locations are shown in figure 7. The mechanism was supported by the tunnel basic sting support system. A photograph of the model installed in the test section is presented in figure 8.

TEST CONDITIONS AND PROCEDURE

Test Conditions

The tests were conducted at Mach numbers of 3.51 and 4.44 and at Reynolds numbers per foot ranging from 2.5×10^6 to 4.2×10^6. During data recording the tunnel stagnation temperature was held constant at approximately 260° F.

Test Procedure

In order to obtain a test point, the tunnel temperature was held constant at approximately 140° F and thermocouple outputs were monitored until equilibrium conditions were reached. At this equilibrium condition a scan of all the thermocouples was taken to determine T_e/T_t. By diverting the flow from the tunnel cooler system, a step increase in tunnel total temperature of approximately 120° F was obtained. Beginning with the initial increase in tunnel temperature the thermocouple outputs were recorded every half second for 45 seconds. These outputs were amplified, digitized, and magnetically recorded by an analog to digital data recording system. Five minutes after the increase in tunnel total temperature a second scan of the thermocouples was obtained, again for the purpose of obtaining the ratio T_e/T_t. As discussed in reference 9, this ratio has been found to be essentially the same at the elevated temperature as it was at the lower temperature; therefore, for the purpose of data reduction, it is assumed to remain constant during the transient period. For these tests the value of T_e/T_t determined prior to the temperature step was used in the data reduction process.

Data Reduction

Heat-transfer coefficients were reduced from the transient skin temperature measurements by using the following relation, which assumes constant temperature through the skin, negligible lateral heat flow, negligible heat flow to the model interior, and no heat losses due to radiation.

$$h = \frac{\tau_{wc} \frac{dT_w}{dt}}{T_e - T_w} \tag{1}$$

Equation (1) may be rewritten in integral form as

$$h = \frac{\tau_{wc} \int_{T_{w,0}}^{T_{w,n}} dT_w}{\int_{t=0}^{t=n} T_e dt - \int_{t=0}^{t=n} T_w dt} \tag{2}$$

Therefore, by assuming T_e/T_t is constant as previously discussed and by evaluating the numerator, the equation may be written as

$$h = \frac{\tau_{wc}\left(T_{w,n} - T_{w,0}\right)}{\frac{T_e}{T_t} \int_{t=0}^{t=n} T_t dt - \int_{t=0}^{t=n} T_w dt} \tag{3}$$

For the purpose of machine calculation the integrals were evaluated by the trapezoidal rule. Thus,

$$\int_{t=0}^{t=n} T dt = \Delta t\left(\frac{1}{2} T_0 + T_1 + T_2 + \cdots T_{m-1} + \frac{1}{2} T_m\right) \tag{4}$$

where Δt is one-half second. A detailed description of this method of data reduction is available in reference 9. Where possible, the heat-transfer coefficients were also determined, with an estimate of the effects of lateral heat flow included, from the following relation:

$$h_c = \frac{\tau_{wc}(T_{w,n} - T_{w,0}) - k\tau \int_{t=0}^{t=n} \left(\frac{\partial^2 T_w}{\partial x_1^2} + \frac{\partial^2 T_w}{\partial y_1^2} \right) dt}{\frac{T_e}{T_t} \int_{t=0}^{t=n} T_t dt - \int_{t=0}^{t=n} T_w dt} \tag{5}$$

The second partial derivatives are evaluated by assuming a linear temperature gradient between adjacent thermocouples.

RESULTS AND DISCUSSION

Fixed-Sweep-Fin Models

The effect of the leading-edge diameter of the fin on the heat-transfer distribution along the fin stagnation line is presented in figure 9 for the three fixed-sweep fins ($\Lambda = 12.87^\circ$) at $M = 3.51$, $R = 4.2 \times 10^6$, and a measured wall-boundary-layer thickness of 6 inches. This figure shows the ratio of the local measured heat-transfer coefficients (with and without conduction corrections) to a theoretical laminar stagnation-line value determined by the method of reference 10. It should be noted that the conduction corrections depend strongly on the fin leading-edge diameter and, although the corrections for the two large fins are considered negligible, they must be considered in the discussion of the 0.75-inch-diameter fin. In general, the heating distribution on the leading edge of the fins consisted of low values of h_s $\left(\text{that is, } \frac{h_s}{h_L} < 1\right)$ near the flat plate, increasing to a peak value at the edge of the boundary layer and then returning to laminar swept-cylinder values in the free stream. The broken line shown across each of the peaks represents theoretical turbulent values for a swept cylinder (determined by the method of ref. 11) divided by the theoretical laminar value. The good agreement with the data indicates that the increased heating in the vicinity of the edge of the boundary layer can be explained by the effects of turbulence. The most pronounced effect of increasing the leading-edge diameter was the increase in the peak heating ratios as predicted by theory and an increase in the area affected by these elevated values.

The heating distribution obtained in the chordwise direction of the three fixed-sweep fins is shown in figure 10 at three spanwise stations for $M = 3.51$ and $R = 4.2 \times 10^6$. The local measured heating rates have been divided by the measured stagnation-line value (corrected for conduction) and are plotted against the parameter s/d for the instrumentation on the nose and against x_c/l for the instrumentation located on the fin side panel. The selection of these two abscissa scales renders geometric similarity to all three fins and permits a better correlation of the experimental data. Presented in the figure is a

theoretical laminar heating distribution for a swept cylinder (ref. 12). Also presented are both laminar and turbulent flat-plate values (ref. 13) for the side panels of the fin having a 3.5-inch-diameter leading edge. The measured distributions obtained on the fin leading edges of all three fins are similar to the theoretical distributions at all three spanwise stations even though the instrumentation at $z/b = 0.111$ and $z/b = 0.333$ is in the presence of the turbulent sidewall boundary layer. Since at $s/d = 0.4$ the magnitude of $\frac{h_c}{(h_c)_s}$ for the two large fins is approximately the same at each of the spanwise stations, the peak heating rates obtained at $z/b = 0.333$ on the stagnation line of the two larger fins shown in figure 9 also occur around the fin leading edge. The heating distributions on the fin side panels at the two inboard stations ($z/b = 0.111$ and $z/b = 0.333$) are associated with a fully turbulent boundary layer, whereas the boundary layer remains laminar at the outboard station ($z/b = 0.611$) to $x_c/l \approx 0.4$. The theoretical turbulent flat-plate distribution divided by $(h_c)_s$ for the 3.5-inch-diameter fin is generally in good agreement with the measured turbulent values at all three stations. The laminar theoretical distribution at the outboard station is in good agreement with the measured laminar values.

Flat Plate

Both the magnitude and distribution of the heat-transfer rates on the flat-plate surface in the vicinity of a protuberance are governed by the extent and nature of the separation and resulting vortex formation originating upstream of the protuberance leading edge. Although no attempts were made in the current investigation to define the vortex formation, the extent of separation and corresponding reverse flow limits upstream of the fin leading edge were determined from the oil-flow photographs in figure 11 and are presented graphically in figure 12 for the three fixed-sweep fins. The distance r is the measured distance from the axis of symmetry of the fin leading edge to the upstream separation line. Also included in the figure is a separation-distance range approximated from the measured heating rates on the variable-sweep fin at a sweep angle of 10°. It should be noted that for the variable-sweep fin the boundary-layer thickness (by method of ref. 14) was only approximately 1/40 of the boundary-layer thickness for the larger fins; however, the measured separation range falls on a smooth curve faired through the origin and the measured points obtained from the larger fins. This, therefore, indicates that for the range of this investigation, the extent of this separation distance is primarily a function of the leading-edge diameter and relatively independent of boundary-layer thickness. Although not presented in the figure, there was also no noticeable effect on the separation distance upstream of the 3.5-inch-diameter fin as a result of varying the Reynolds number by a factor of 2 at $M = 3.51$ or as a result of increasing the Mach number from 3.51 to 4.44 (fig. 11(b)).

The measured flat-plate heating distributions in the 6-inch boundary layer upstream of the fin leading edge are presented in figure 13 for the three fixed-sweep fins at Mach numbers of 3.51 and 4.44 and Reynolds numbers per foot of approximately 2.6×10^6 and 4.2×10^6. Also presented is the measured distribution obtained on the flat-plate surface in a 0.155-inch boundary layer

upstream of the variable-sweep fin at a sweep angle of 10° for $M = 3.51$ and $R = 4.2 \times 10^6$. The local measured heat-transfer coefficients presented in figure 13 have been nondimensionalized for the 6-inch boundary layer by the measured heating rates obtained on the flat plate alone, and for the 0.155-inch boundary layer by a theoretical distribution determined from the turbulent theory of reference 13; these ratios are plotted against the nondimensional surface length r/d. At $M = 3.51$ and for both Reynolds numbers, there is no apparent deviation from the heating rates for the plate alone upstream of the separation boundary determined from figure 11. Although there is scatter of the data within the separation region, a fair correlation of the experimental data is obtained for all models with no apparent trend in the parameter h/h_o with either varying leading-edge diameter or Reynolds number. Within the separated region the values of h/h_o increase rapidly from approximately 1 at $r/d \approx 3$ to approximately 4 at $r/d \approx 0.5$. Increasing the Mach number to 4.44 (fig. 13(b)) had a very small effect on h/h_o except at the station nearest the fin leading edge where an increase in the ratio occurred and was most predominant for the 3.5-inch-diameter fin. There was also an indication of an increase in the heating ratio at this station with decreasing Reynolds number; however, these data are too limited to be conclusive.

Presented in figure 14 are the heating ratios obtained on the flat-plate surface for $\delta = 6$ inches at two stations (normal to the fin plane of symmetry) downstream of the leading edges of the three fixed-sweep fins. For $x = 20$ inches, which corresponds to a range of r/d from -0.5 to -4.6 for the three fins, the heating distributions are a strong function of the leading-edge diameter. In general, the distribution at $x = 20$ inches consists of an increase in the heating rates for decreasing values of y/d except for the instrumentation located in the immediate vicinity of the two large-diameter fins where a decrease in heating is indicated. This decrease could in part be due to heat losses by conduction to the cooler skin under the fin; however, estimates of this loss do not account for the entire indicated decrease. The maximum value of the peak heating rates occurring in the vicinity of the corner region decreases with decreasing leading-edge diameter (increasing r/d). At the aft station ($x = 32$ inches) which corresponds to a range of r/d from -4.0 to -20.6, there is no apparent trend in the data with varying r/d.

Variable-Sweep-Fin Model

The effect of leading-edge sweep, for the 0.25-inch-diameter fin, on the heating distribution over the flat-plate surface is shown in figure 15 for a Mach number of 3.51, Reynolds number of 4.2×10^6, and angles of sweep from 0° through 69°. At each value of sweep, data are presented for six spanwise stations. Also presented in the figure is a theoretical turbulent flat-plate heating distribution (ref. 13) based on free-stream conditions. The measured flat-plate distribution at $y/d = 0$ indicates a fully developed turbulent boundary layer at $r/d \approx 6.5$ throughout the range of sweep angles. For $\Lambda = 0°$ most of the instrumented flat plate downstream of $r/d \approx 3.5$ is affected by the interference region. Along the plate center line ($y/d = 0$) the maximum measured heating rates would be expected to occur at $r/d \approx 0.5$ (based on the results presented in fig. 13); however, because of the small size of the model, instrumentation could not be located at $r/d < 1.5$. The data indicate that as

the value of y/d increases the location of peak heating (which decreases in magnitude) moves downstream as would be expected. Increasing sweep angle resulted in a decrease in both the area affected by the interference region and the magnitude of the heating rates within this interference region. The effects of sweep angle on the heating distribution are further illustrated in figure 16, where the local heating rates are plotted against the angle of sweep for the entire range of y/d at three stations downstream of the flat-plate leading edge. At the station upstream of the fin leading edge, $r/d = 1.5$, the heating rate located in the plane of symmetry of the fins ($y/d = 0$) decreases with increasing sweep from a value approximately twice the theoretical flat-plate value to approximately the same magnitude as the flat-plate value at a sweep angle of 40°. At this sweep angle the flow interference region has apparently moved downstream of $r/d = 1.5$, and therefore further increases in sweep have no effect on the measured values. The magnitude of the heating rates on the plate decreases with increasing distance from the fin plane of symmetry and generally approaches the magnitude of the undisturbed plate heating rates even at the lowest angles of sweep. The instrumentation at the stations located at $y/d > 3$ is apparently outside the interference region (for $r/d = 1.5$) throughout the complete range of sweep angles. Similar heating distributions are shown at $r/d = -0.5$ and $r/d = -4.5$ with a general increase in the area affected by the fin with decreasing values of r/d. Through the range of sweep from 0° to 40° the sweep has a large effect on the heating distribution throughout the range of r/d for $y/d \leqq 5$, whereas for angles from 40° to 69° the interference region is apparently confined to the immediate fin—flat-plate corner ($y/d \leqq 1$).

The flat-plate heating distribution throughout the range of sweep angles for $R \approx 2.5 \times 10^6$ and $M = 3.51$ is presented in figure 17 for the 0.25-inch-diameter leading-edge fin. At each value of sweep, data are presented for six spanwise stations. The fixed transition strip failed to trip the boundary layer at this Reynolds number, and it apparently remained laminar outside the fin interference region to the most aft instrumentation location throughout the range of sweep angles. The trend of the heating distribution within the interference region is very similar to that obtained at the higher Reynolds number. At the lower sweep angles and small values of y/d the peak heating rates are approximately of the same magnitude as those obtained at the higher Reynolds number, which indicates transitional or turbulent flow within the interference region. Due to the transitional flow within the interference region, it is difficult to distinguish between the effects of transition and interference; however, heating rates greater than the laminar values are indicated by the experimental results throughout the range of sweep angles for $y/d \leqq 2$.

CONCLUDING REMARKS

Heating distributions have been obtained on three fixed-sweep fins (12.87°) of different leading-edge diameters partially submerged in a turbulent boundary layer, as well as on the flat-plate surface adjacent to these fins. Heating rates have also been obtained on a flat plate adjacent to a fin at sweep angles varying from 0° to 69°.

The heating rates obtained on the leading edge of the fins outboard of the sidewall boundary-layer effects are in good agreement with laminar theory. The maximum stagnation-line values obtained in the region subjected to the flow of the turbulent sidewall boundary layer are in good agreement with turbulent theory. The variation of separation distance on the flat plate upstream of the fin leading edge with diameter was found to be approximately linear and relatively independent of boundary-layer thickness. The ratio of the heat-transfer coefficients obtained on the center line of the flat plate with the fins mounted to those obtained on the flat plate alone, h/h_o, upstream of the stagnation line of the fins investigated tends to fall on a single general curve when plotted against the distance from the center line of the fin leading edge in diameters, r/d. In general, $h/h_o \approx 1$ for $r/d > 2.5$ and increases asymptotically, within the span of instrumentation, as the fin leading edge is approached. The correlation of data obtained from the 0.155-inch and the 6-inch boundary layer, using the parameters r/d and h/h_o, indicates that boundary-layer thickness has relatively little, if any, effect on the ratio h/h_o in the interference region.

In general, increasing sweep resulted in a decrease in both the area affected by interference on the flat plate and the magnitude of the heating rates within this interference region. At the high Reynolds number (4.2×10^6), where the boundary layer was turbulent, the maximum measured heating rate nearest the fin, upstream of the fin stagnation line $(r/d = 1.5)$, decreases from approximately twice the theoretical turbulent flat-plate value at $\Lambda = 0^\circ$ to the undisturbed value at $\Lambda = 40^\circ$. Further increases in sweep had only a slight effect on the heating distribution within the entire interference region. At the low Reynolds number (2.5×10^6) the boundary layer remained laminar outside the fin interference region. However, within the interference region the heating rates at the lower sweep angles were of approximately the same magnitude as those obtained at the high Reynolds number, indicating transitional or turbulent flow. Due to the apparent transitional flow in this region, the effects of sweep are significant on the flat-plate heating rates in the vicinity of the fin throughout the tested range of sweep.

Langley Research Center,
National Aeronautics and Space Administration,
Langley Station, Hampton, Va., March 3, 1964.

REFERENCES

1. Burbank, Paige B., Newlander, Robert A., and Collins, Ida K.: Heat-Transfer and Pressure Measurements on a Flat-Plate Surface and Heat-Transfer Measurements on Attached Protuberances in a Supersonic Turbulent Boundary Layer at Mach Numbers of 2.65, 3.51, and 4.44. NASA TN D-1372, 1962.

2. Bloom, Martin H., and Pallone, Adrian: Heat Transfer to Surfaces in the Neighborhood of Protuberances in Hypersonic Flow. WADC TN 57-95, ASTIA Doc. No. AD 118138, U.S. Air Force, Aug. 1957.

3. Burbank, Paige B., and Strass, H. Kurt: Heat Transfer to Surfaces and Protuberances in a Supersonic Turbulent Boundary Layer. NACA RM L58E01a, 1958.

4. Newlander, Robert A.: Effect of Shock Impingement on the Distribution of Heat-Transfer Coefficients on a Right Circular Cylinder at Mach Numbers of 2.65, 3.51, and 4.44. NASA TN D-642, 1961.

5. Yip, P. S.: Test Report for Phase III of the Aerodynamic Heating Test at the NASA Langley Unitary Plan Wind Tunnel. Rep. No. ZT-7-027 (Contract No. AF04(645)-4), Convair/Astronautics, July 2, 1959.

6. Wisniewski, Richard J.: Turbulent Heat-Transfer Coefficients in the Vicinity of Surface Protuberances. NASA MEMO 10-1-58E, 1958.

7. Hiers, R. S.: Heat Transfer to Protuberances Partially Immersed in a Hypersonic, Turbulent Boundary Layer. AEDC-TDR-62-66 (Contract No. AF40(600)-800 S/A 24(61-73)), Arnold Eng. Dev. Center, Apr. 1962.

8. Anon.: Manual for Users of the Unitary Plan Wind Tunnel Facilities of the National Advisory Committee for Aeronautics. NACA, 1956.

9. Burbank, Paige B., and Hodge, B. Leon: Distribution of Heat Transfer on a 10° Cone at Angles of Attack From 0° to 15° for Mach Numbers of 2.49 to 4.65 and a Solution to the Heat-Transfer Equation That Permits Complete Machine Calculations. NASA MEMO 6-4-59L, 1959.

10. Reshotko, Eli, and Beckwith, Ivan E.: Compressible Laminar Boundary Layer Over a Yawed Infinite Cylinder With Heat Transfer and Arbitrary Prandtl Number. NACA Rep. 1379, 1958. (Supersedes NACA TN 3986.)

11. Beckwith, Ivan E., and Gallagher, James J.: Local Heat Transfer and Recovery Temperatures on a Yawed Cylinder at a Mach Number of 4.15 and High Reynolds Numbers. NASA TR R-104, 1961. (Supersedes NASA MEMO 2-27-59L.)

12. Goodwin, Glen, Creager, Marcus O., and Winkler, Ernest L.: Investigation of Local Heat-Transfer and Pressure Drag Characteristics of a Yawed Circular Cylinder at Supersonic Speeds. NACA RM A55H31, 1956.

13. Van Driest, E. R.: The Problem of Aerodynamic Heating. Aero. Eng. Rev., vol. 15, no. 10, Oct. 1956, pp. 26-41.

14. Tucker, Maurice: Approximate Calculation of Turbulent Boundary-Layer Development in Compressible Flow. NACA TN 2337, 1951.

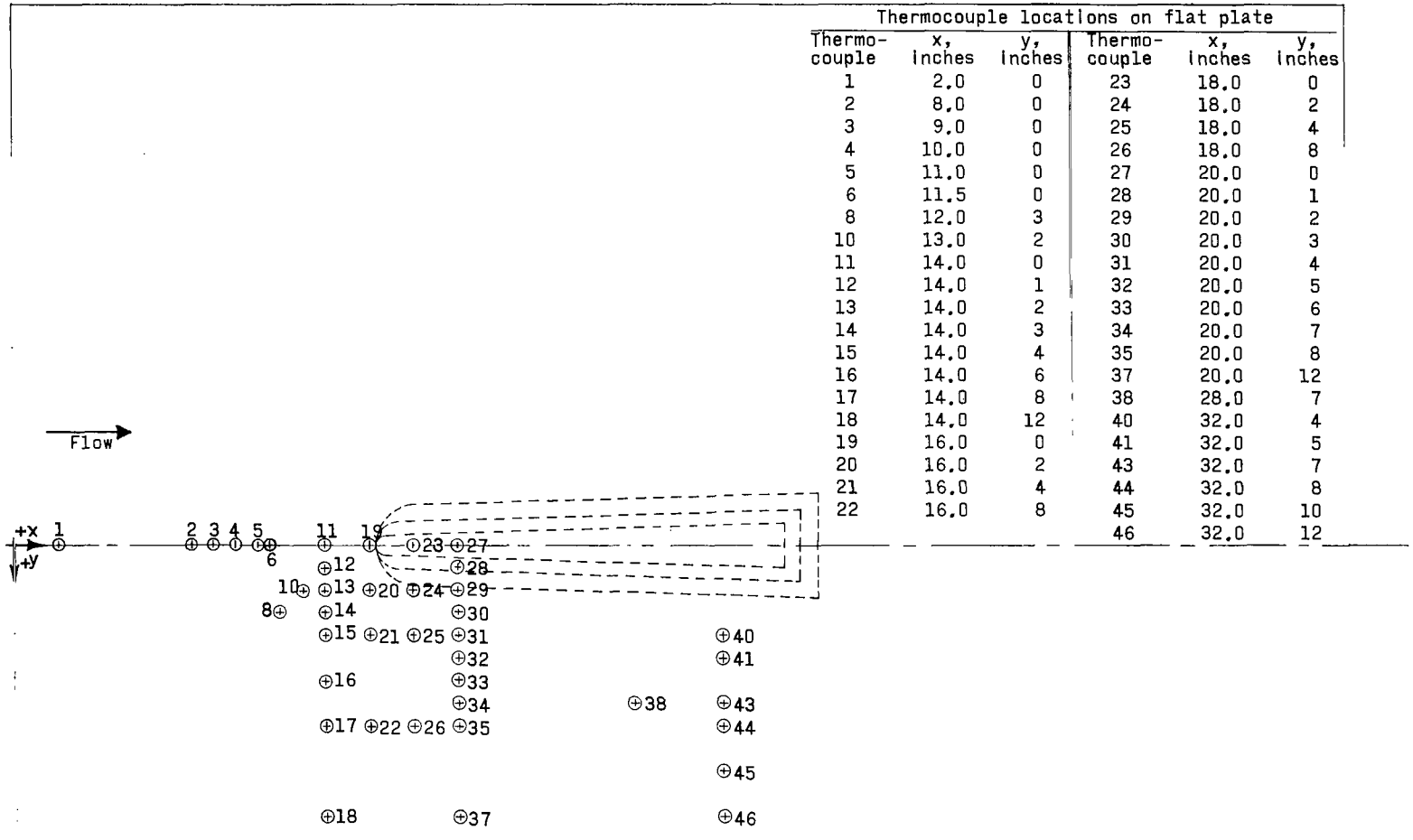

Thermocouple locations on flat plate

Thermocouple	x, inches	y, inches	Thermocouple	x, inches	y, inches
1	2.0	0	23	18.0	0
2	8.0	0	24	18.0	2
3	9.0	0	25	18.0	4
4	10.0	0	26	18.0	8
5	11.0	0	27	20.0	0
6	11.5	0	28	20.0	1
8	12.0	3	29	20.0	2
10	13.0	2	30	20.0	3
11	14.0	0	31	20.0	4
12	14.0	1	32	20.0	5
13	14.0	2	33	20.0	6
14	14.0	3	34	20.0	7
15	14.0	4	35	20.0	8
16	14.0	6	37	20.0	12
17	14.0	8	38	28.0	7
18	14.0	12	40	32.0	4
19	16.0	0	41	32.0	5
20	16.0	2	43	32.0	7
21	16.0	4	44	32.0	8
22	16.0	8	45	32.0	10
			46	32.0	12

Figure 1.- Thermocouple locations and relative location of fixed-sweep fins on tunnel-sidewall test plate.

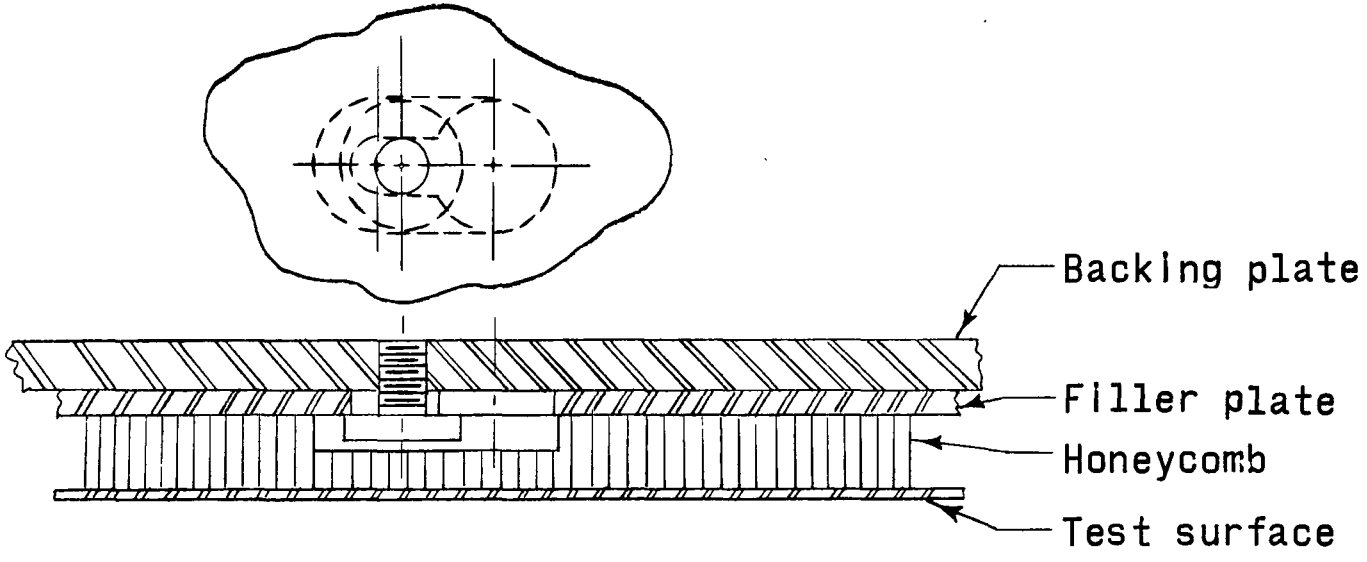

Figure 2.- Cross section of sandwich-type construction.

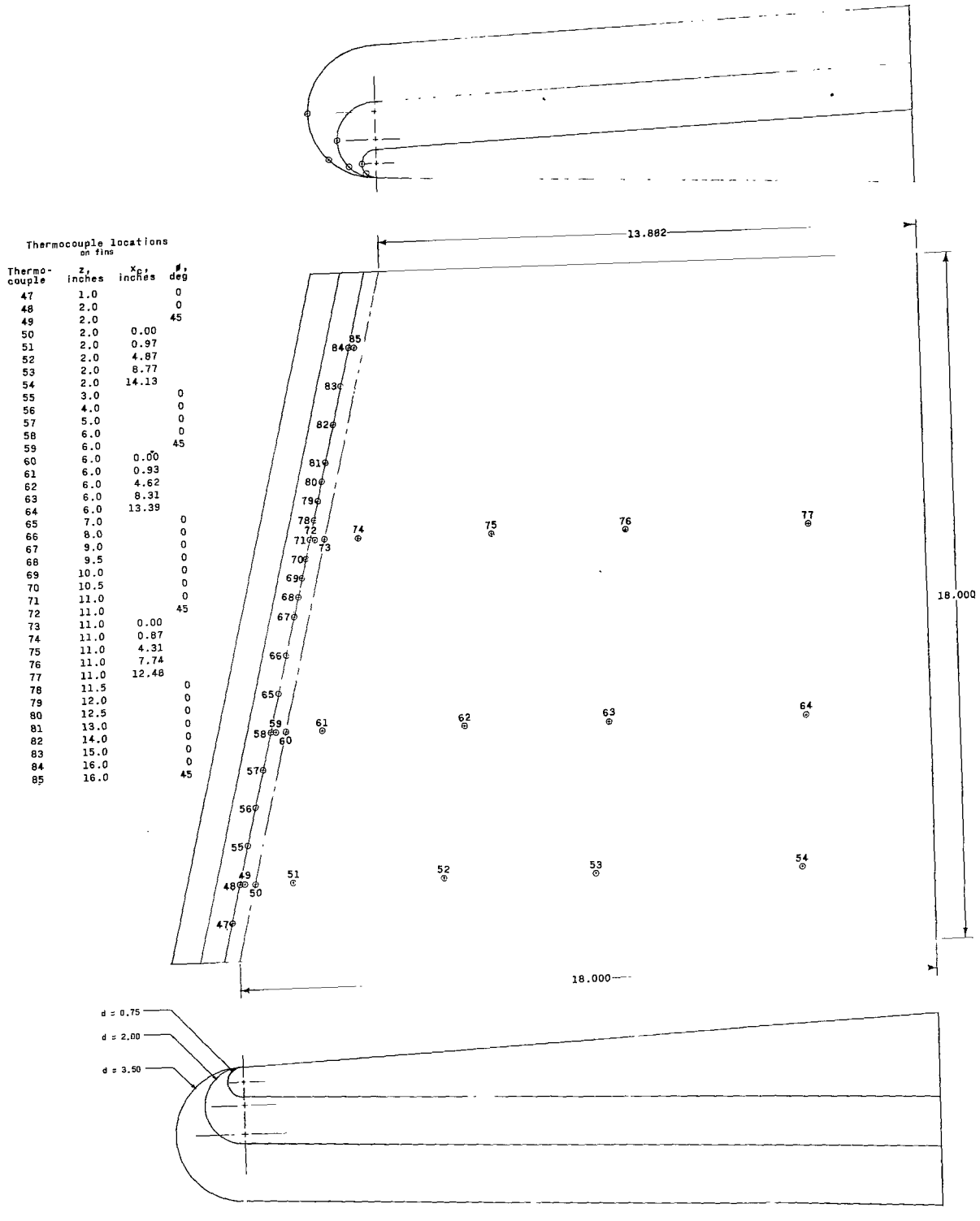

Figure 3.- Thermocouple locations on fixed-sweep fins. (All dimensions are in inches unless otherwise indicated.)

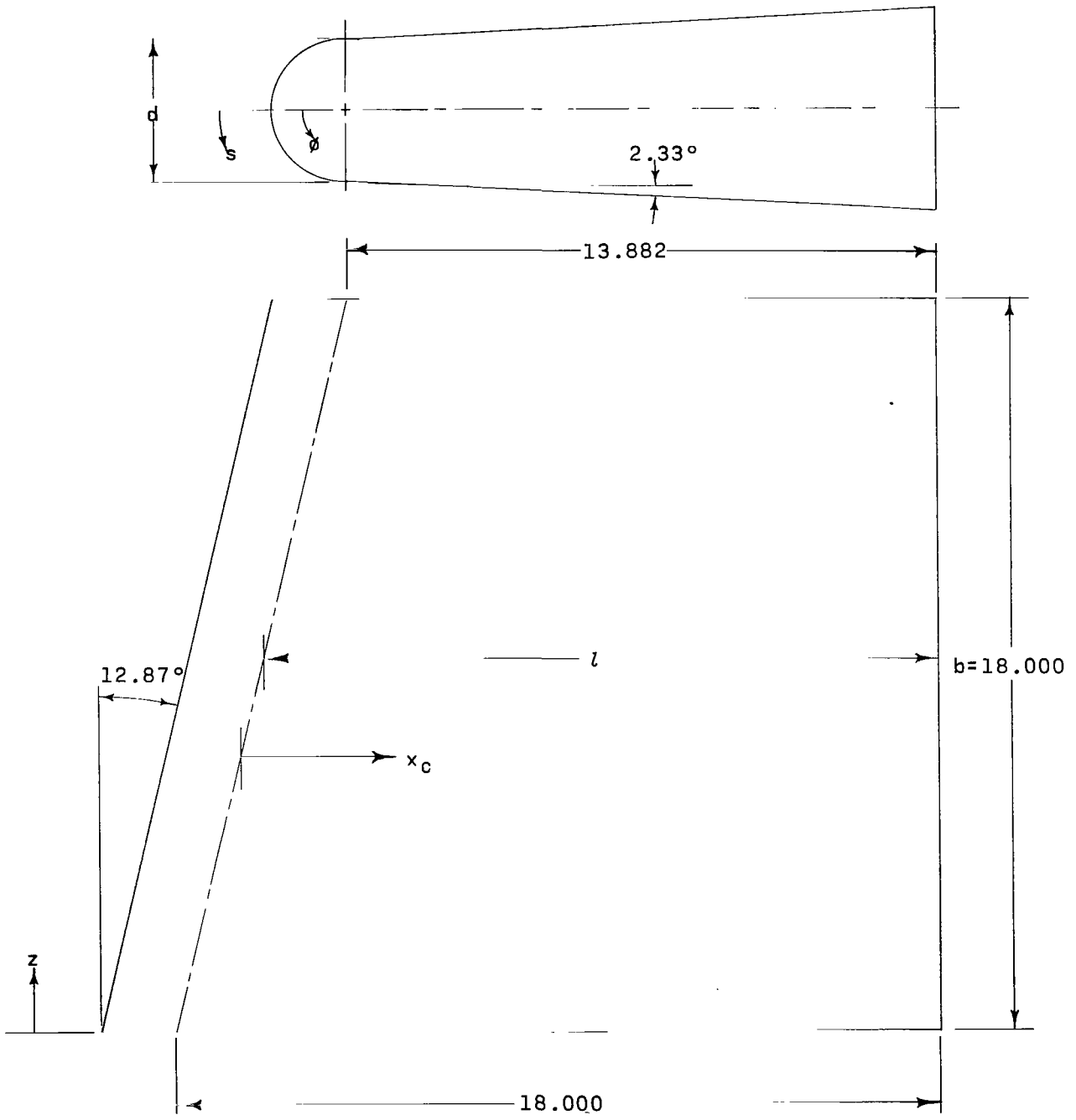

Figure 4.- Geometric characteristics of fixed-sweep fins. (All dimensions are in inches unless otherwise indicated.)

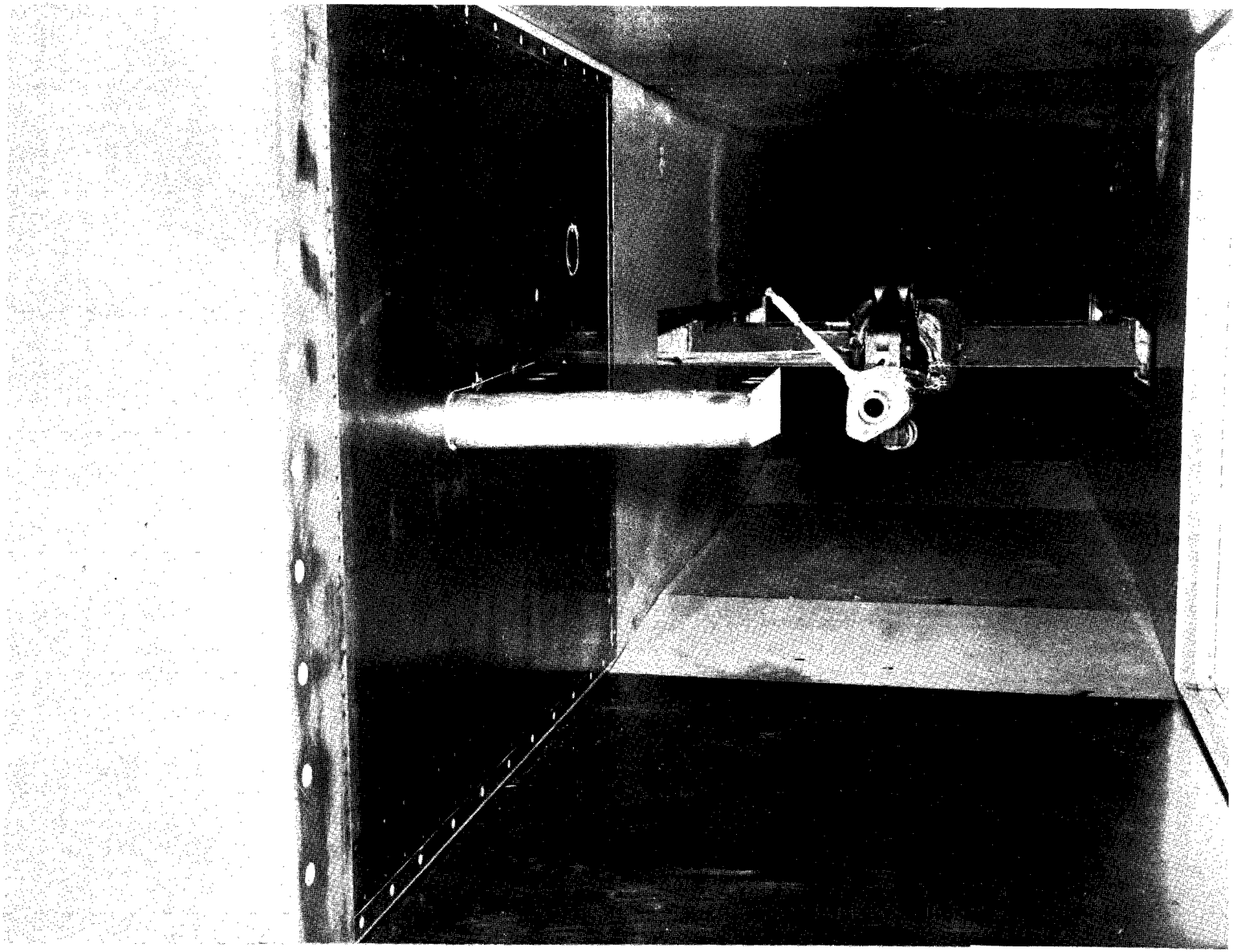

L-62-4015

Figure 5.- Photograph of fixed-sweep fin having 3.5-inch leading-edge diameter installed in test section.

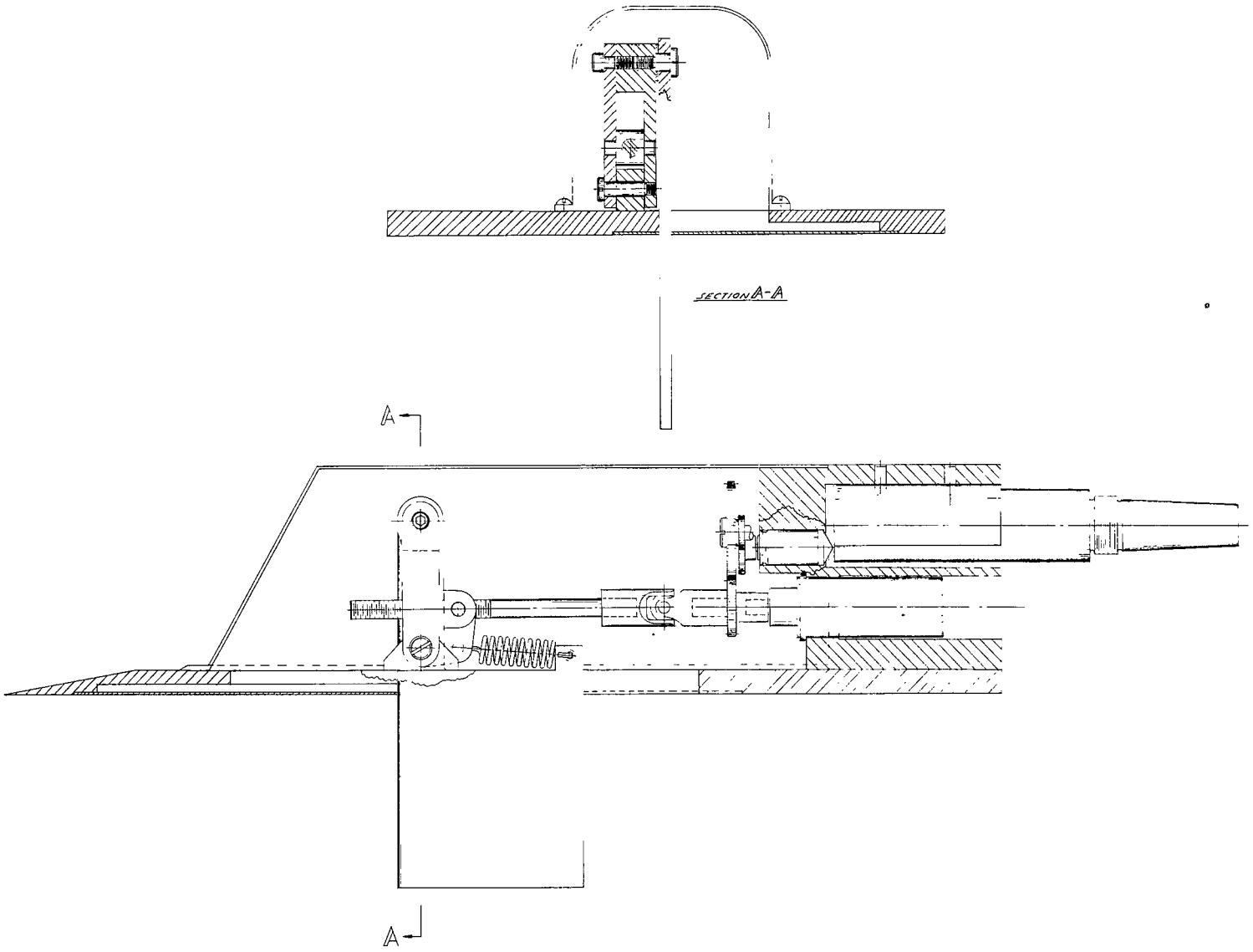

Figure 6.- General arrangement of model having variable-sweep fin.

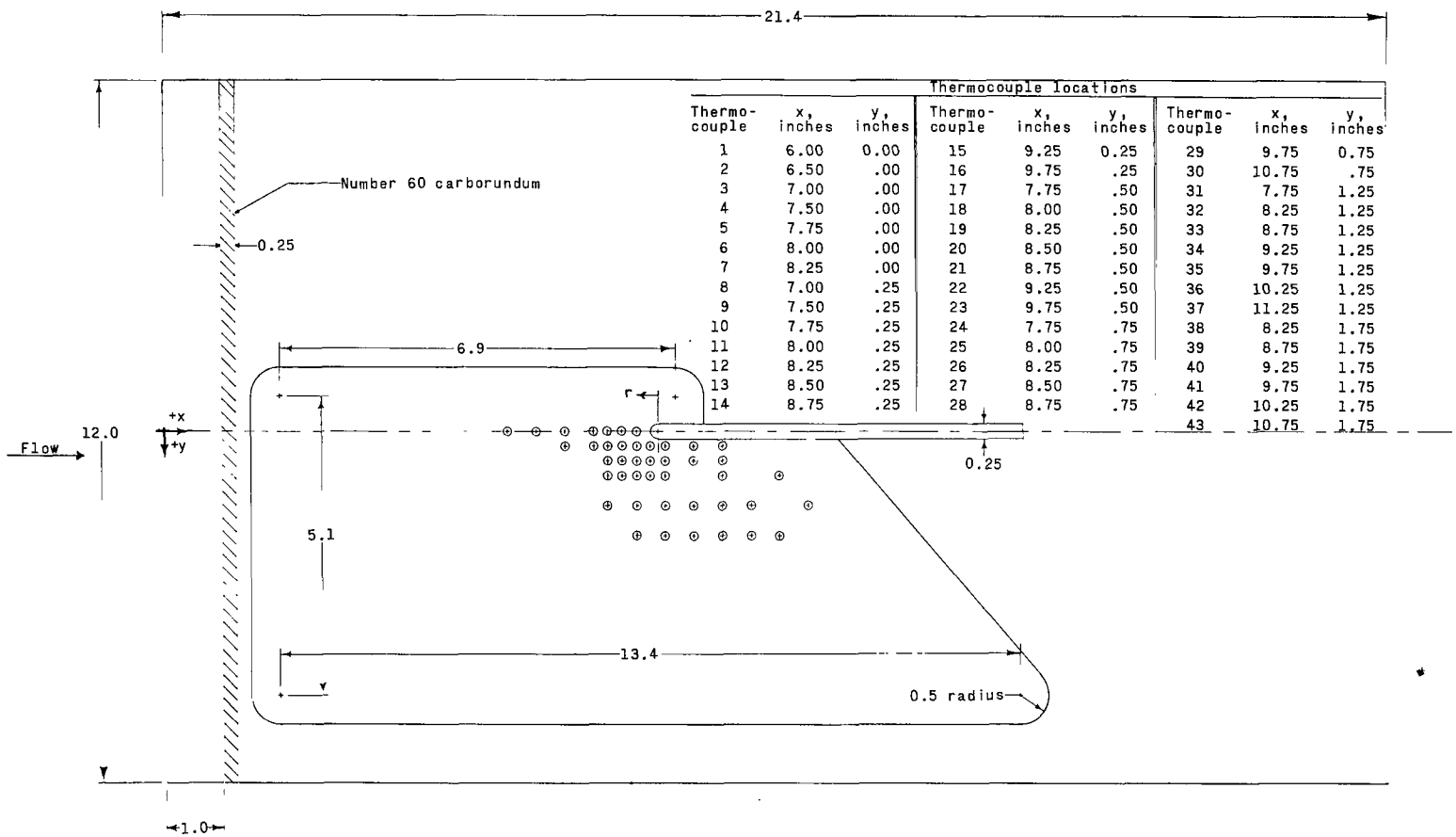

Thermocouple locations

Thermocouple	x, inches	y, inches	Thermocouple	x, inches	y, inches	Thermocouple	x, inches	y, inches
1	6.00	0.00	15	9.25	0.25	29	9.75	0.75
2	6.50	.00	16	9.75	.25	30	10.75	.75
3	7.00	.00	17	7.75	.50	31	7.75	1.25
4	7.50	.00	18	8.00	.50	32	8.25	1.25
5	7.75	.00	19	8.25	.50	33	8.75	1.25
6	8.00	.00	20	8.50	.50	34	9.25	1.25
7	8.25	.00	21	8.75	.50	35	9.75	1.25
8	7.00	.25	22	9.25	.50	36	10.25	1.25
9	7.50	.25	23	9.75	.50	37	11.25	1.25
10	7.75	.25	24	7.75	.75	38	8.25	1.75
11	8.00	.25	25	8.00	.75	39	8.75	1.75
12	8.25	.25	26	8.25	.75	40	9.25	1.75
13	8.50	.25	27	8.50	.75	41	9.75	1.75
14	8.75	.25	28	8.75	.75	42	10.25	1.75
						43	10.75	1.75

Figure 7.- Thermocouple locations and geometric characteristics of model having variable-sweep fin.
(All dimensions are in inches unless otherwise indicated.)

L-62-4034

Figure 8.- Photograph of model having variable-sweep fin installed in test section.

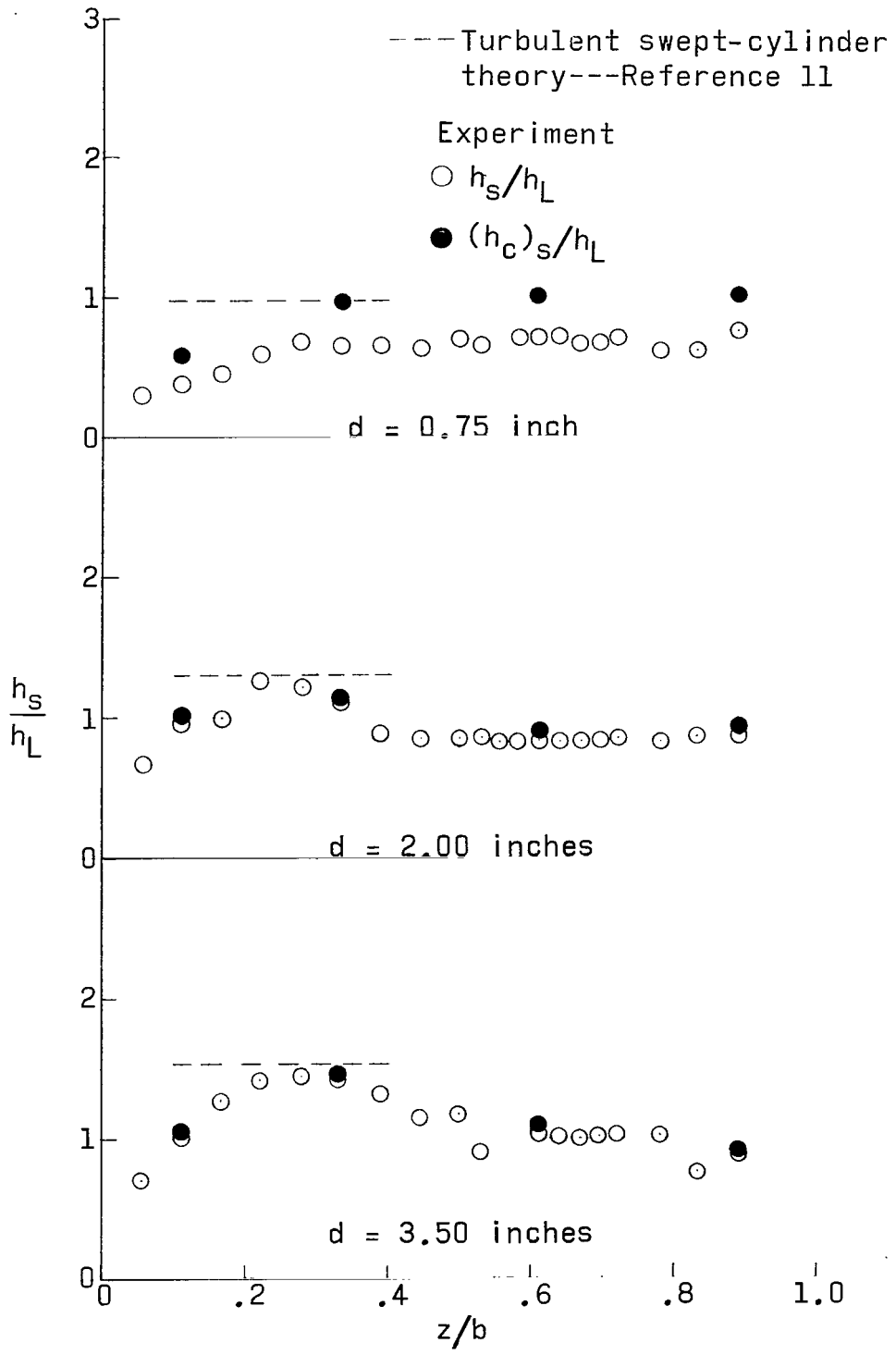

Figure 9.- Effect of leading-edge diameter on stagnation-line heating distribution of fixed-sweep fins. M = 3.51; R $\approx 4.2 \times 10^6$.

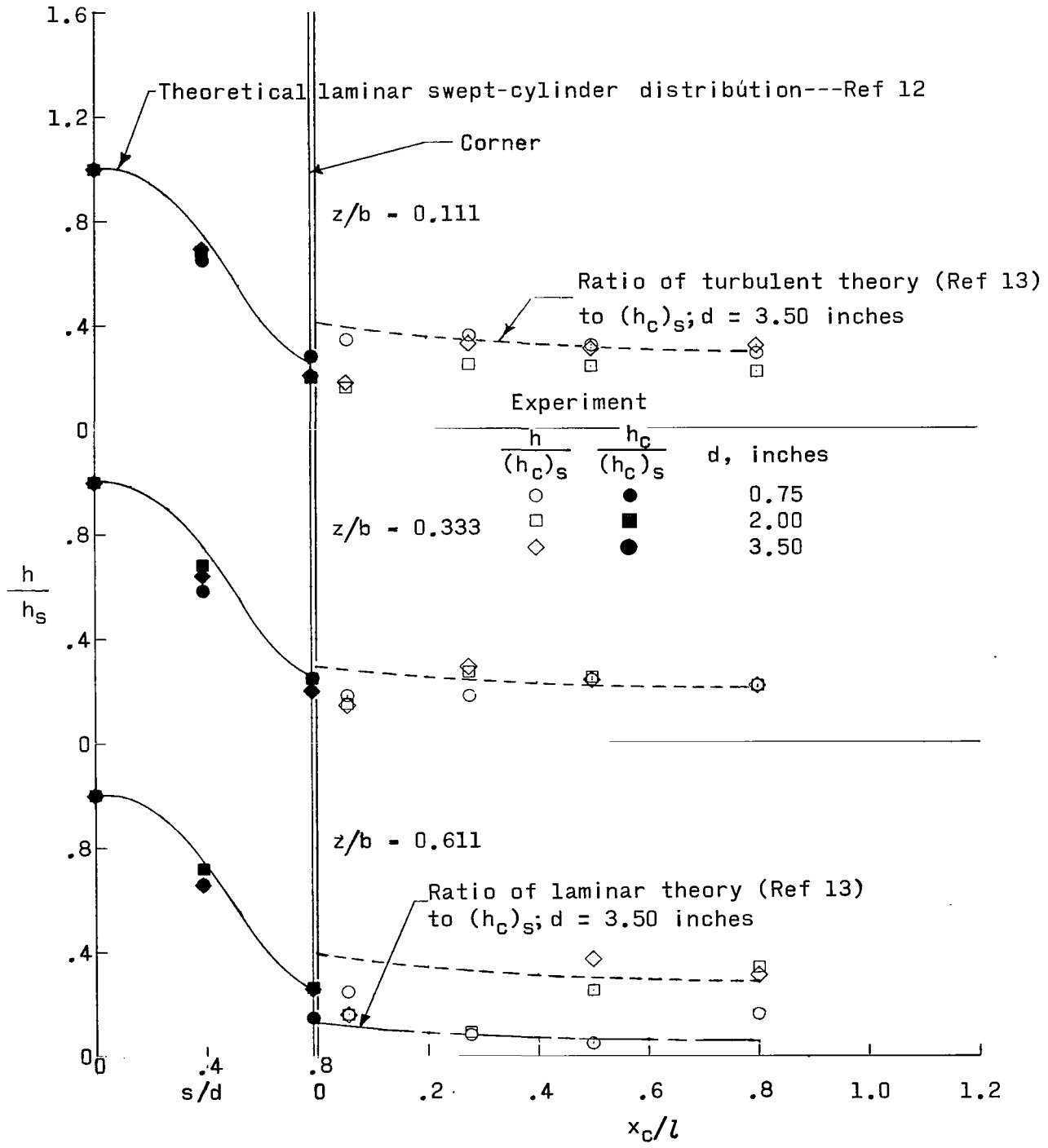

Figure 10.- Effect of leading-edge diameter on chordwise heating distribution of fixed-sweep fins. M = 3.51; R ≈ 4.2×10^6.

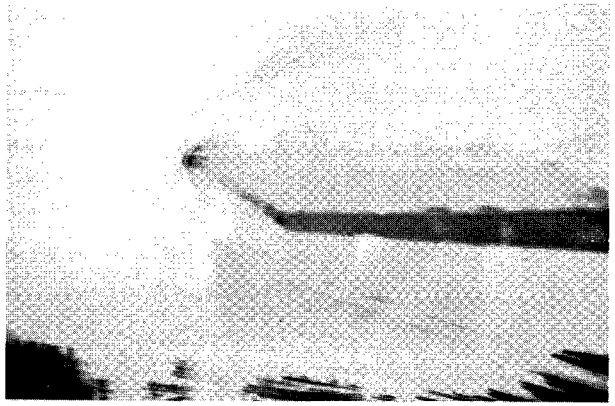

d = 0.75 inch; R ≈ 1.2×10^6

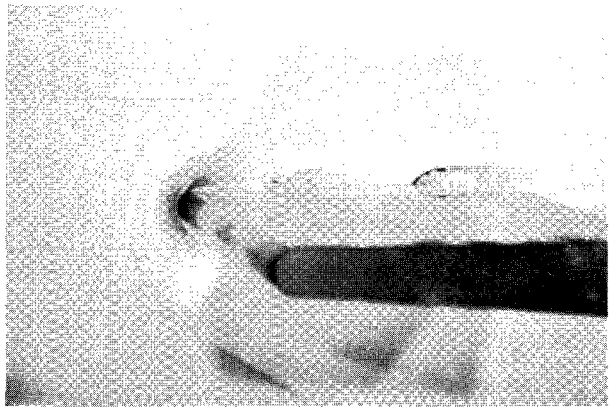

d = 2.00 inches; R ≈ 2.4×10^6

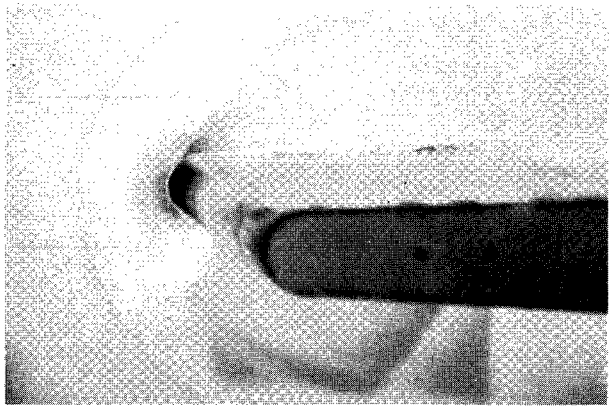

d = 3.50 inches; R ≈ 2.4×10^6

(a) M = 3.51. L-64-428

Figure 11.- Oil-flow photographs of model having fixed-sweep fin.

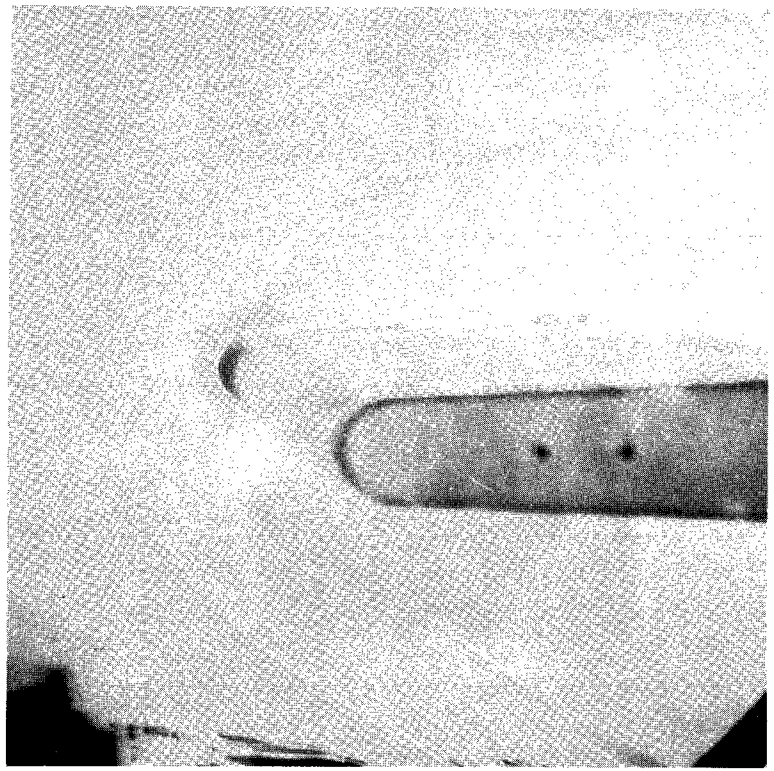

M = 3.51; R ≈ 1.2 x 10^6

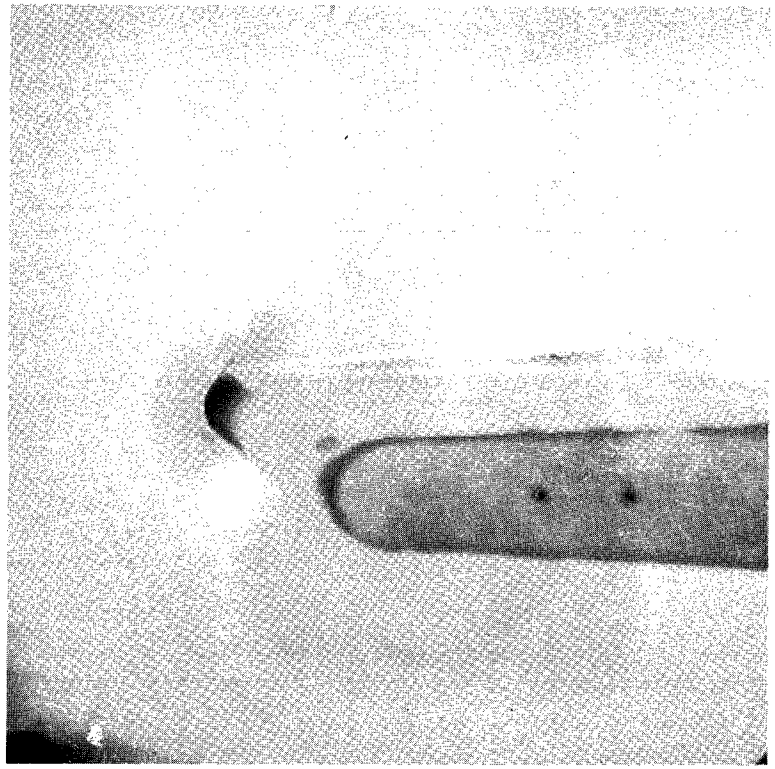

M = 4.44; R ≈ 4.5 x 10^6

(b) d = 3.50. L-64-429

Figure 11.- Concluded.

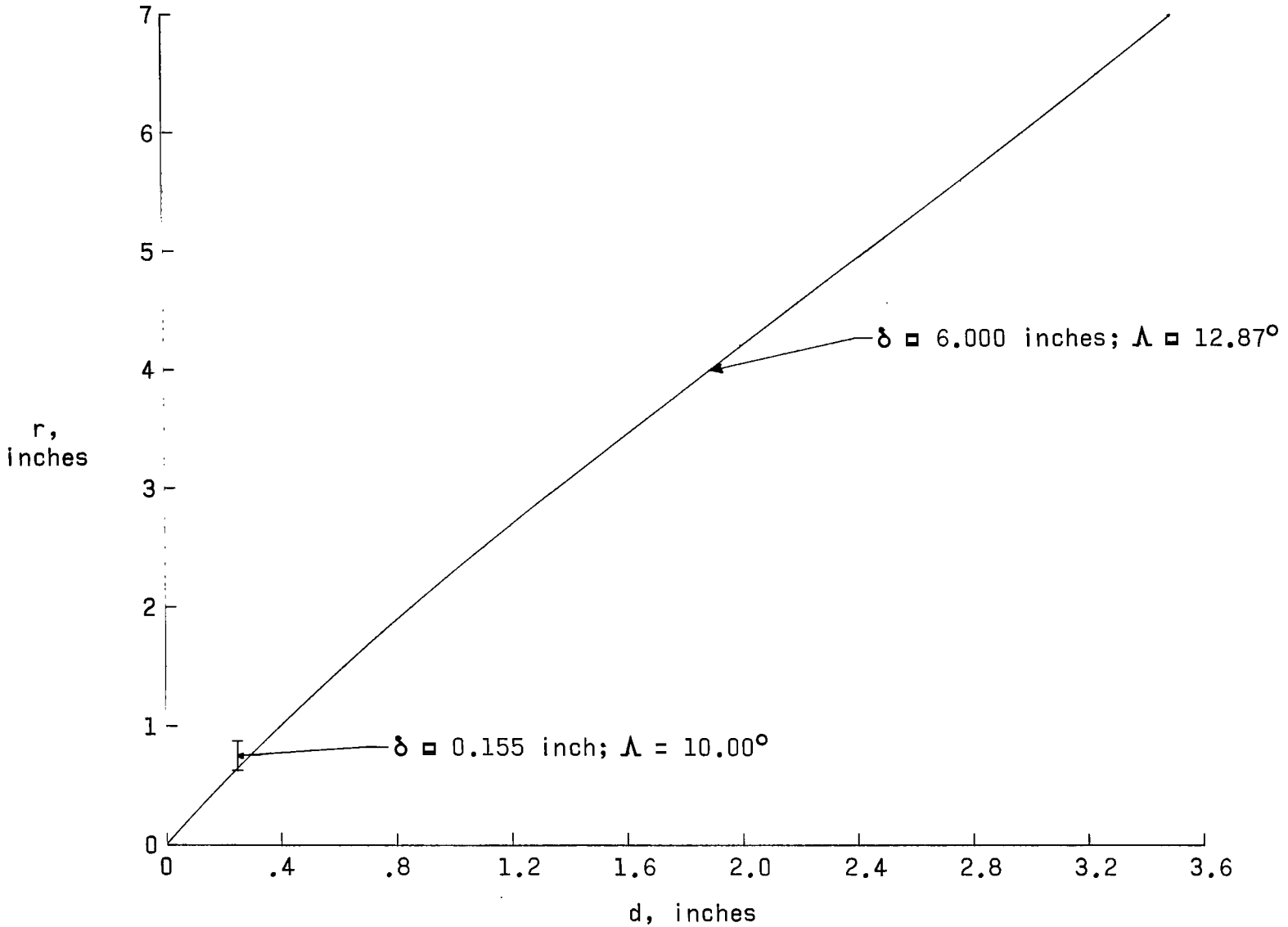

Figure 12.- Effect of fin leading-edge diameter and boundary-layer thickness on separation distance upstream of fin. $M = 3.51$; $R \approx 4.2 \times 10^6$.

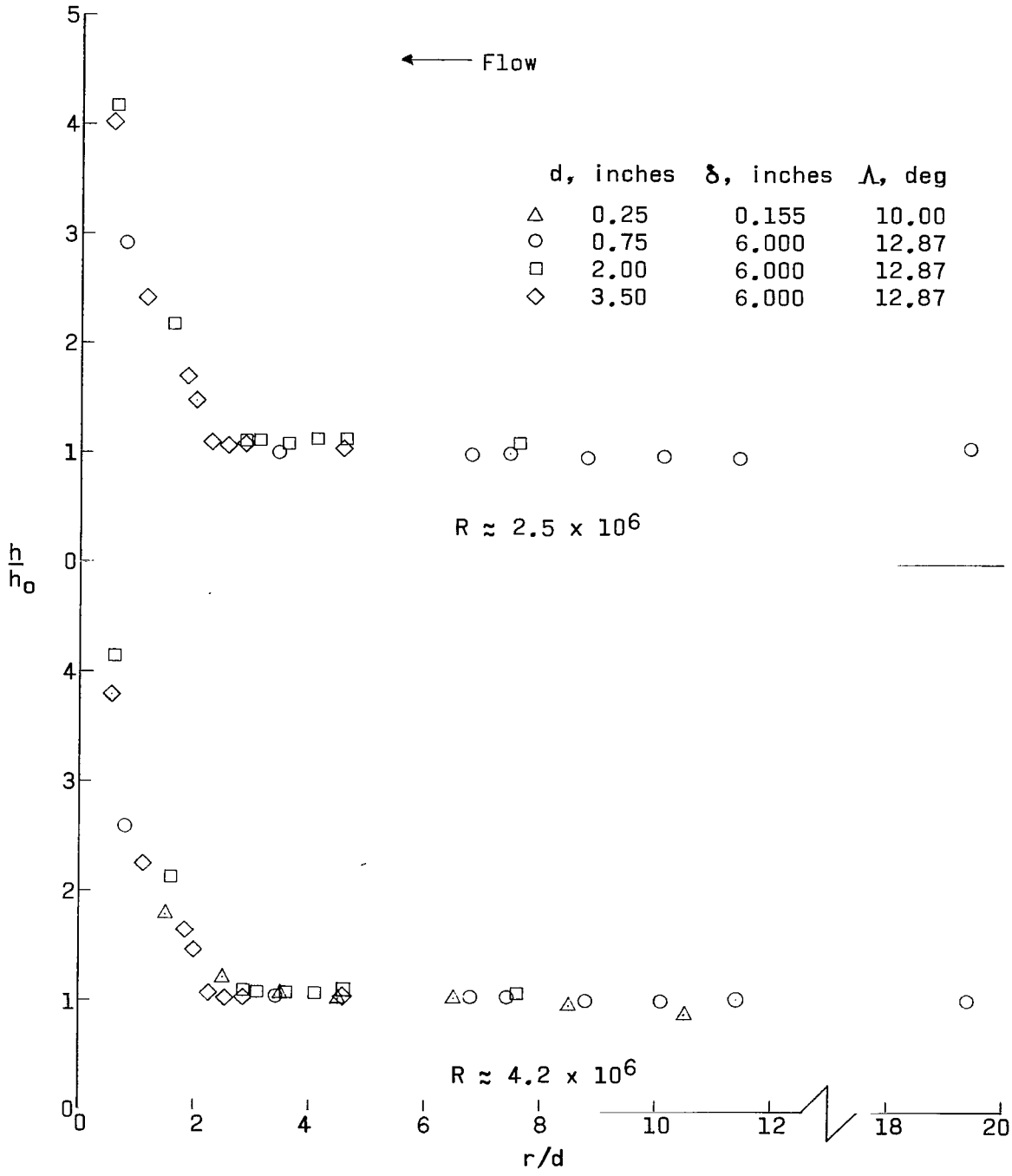

(a) M = 3.51.

Figure 13.- Effect of fin leading-edge diameter and boundary-layer thickness on adjacent-surface heating distribution upstream of fin stagnation line.

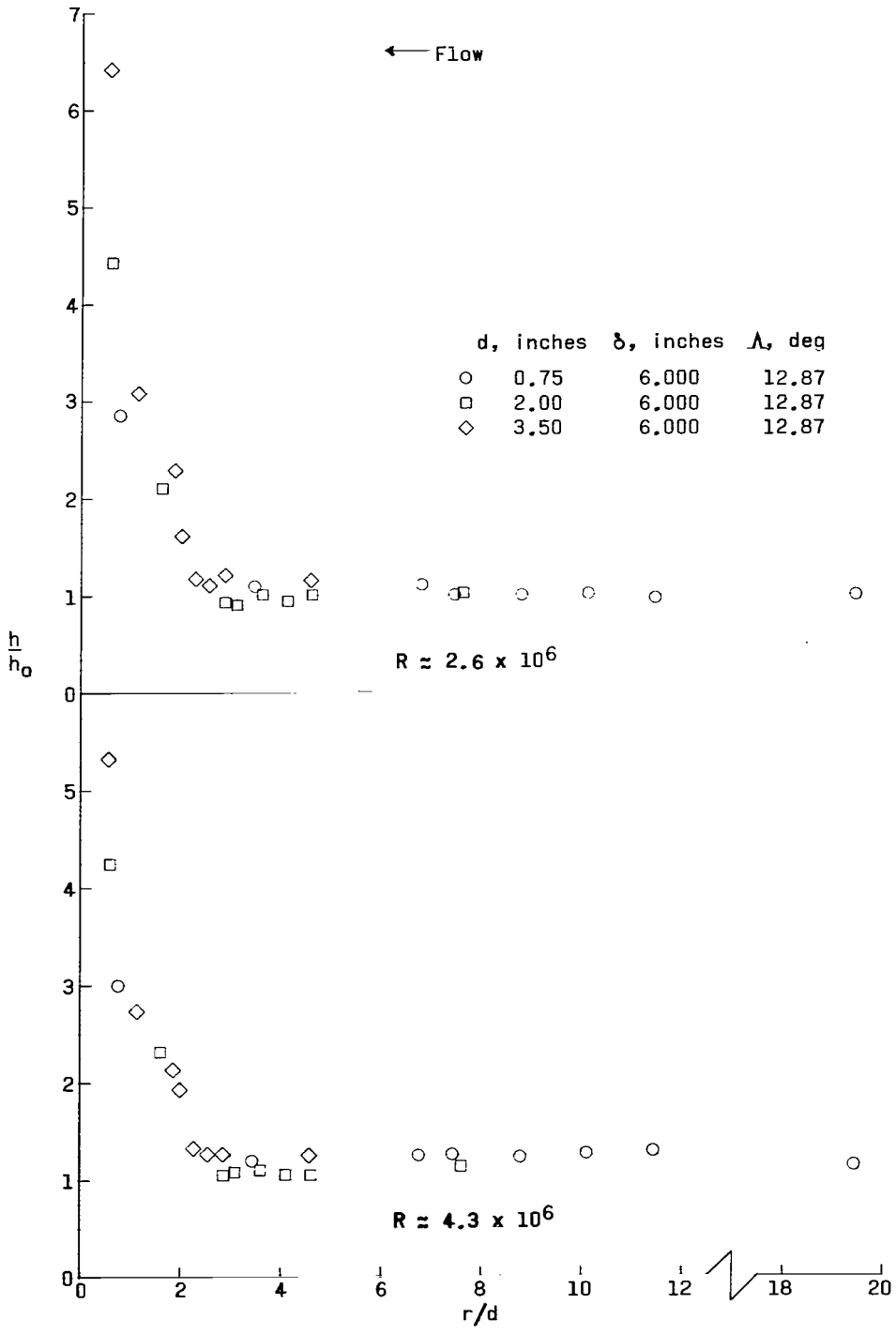

(b) M = 4.44.

Figure 13.- Concluded.

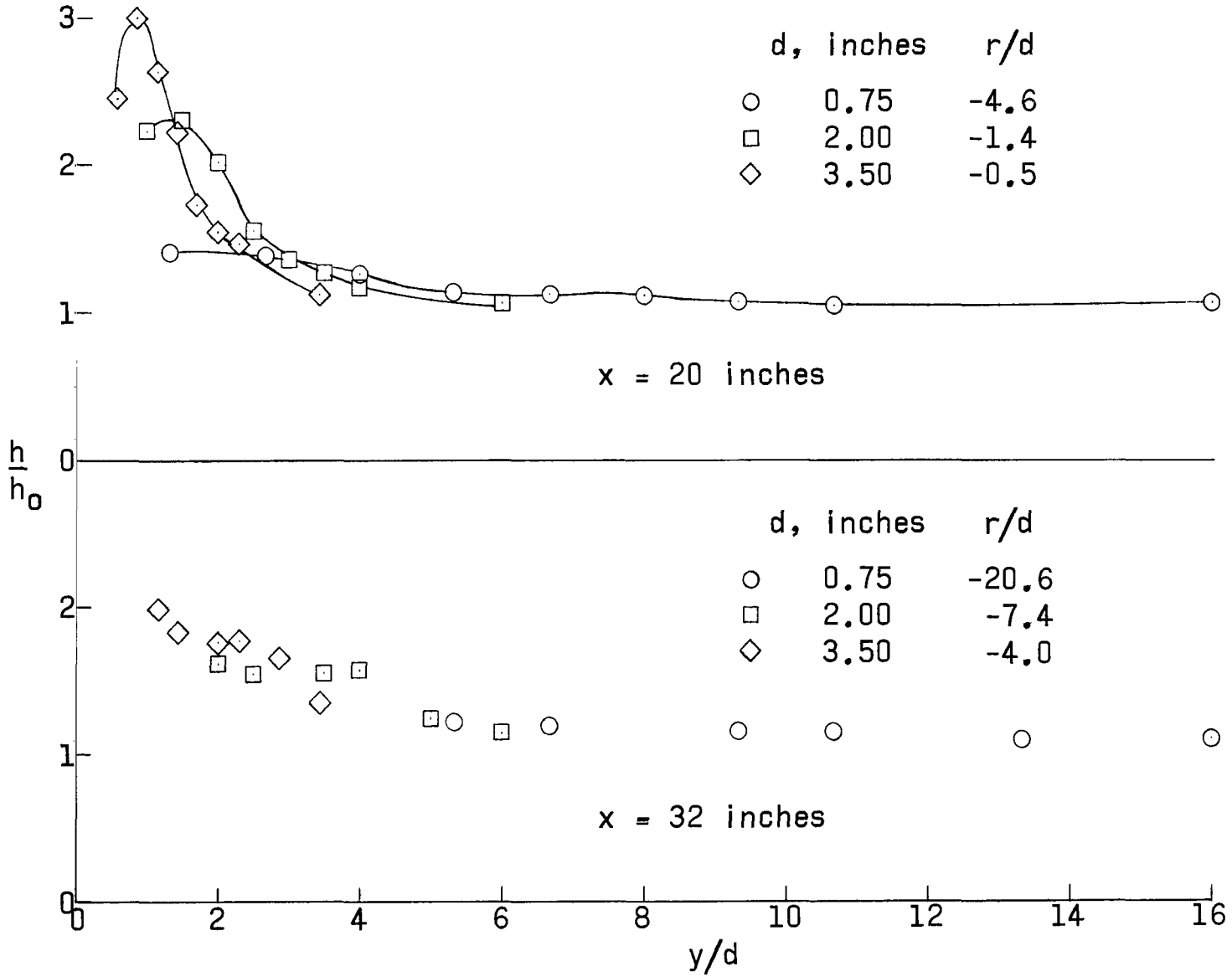

Figure 14.- Effect of fin leading-edge diameter on flat-plate heating distribution normal to fin plane of symmetry downstream of fin leading edge. $M = 3.51$; $R \approx 4.2 \times 10^6$; $\delta = 6$ inches.

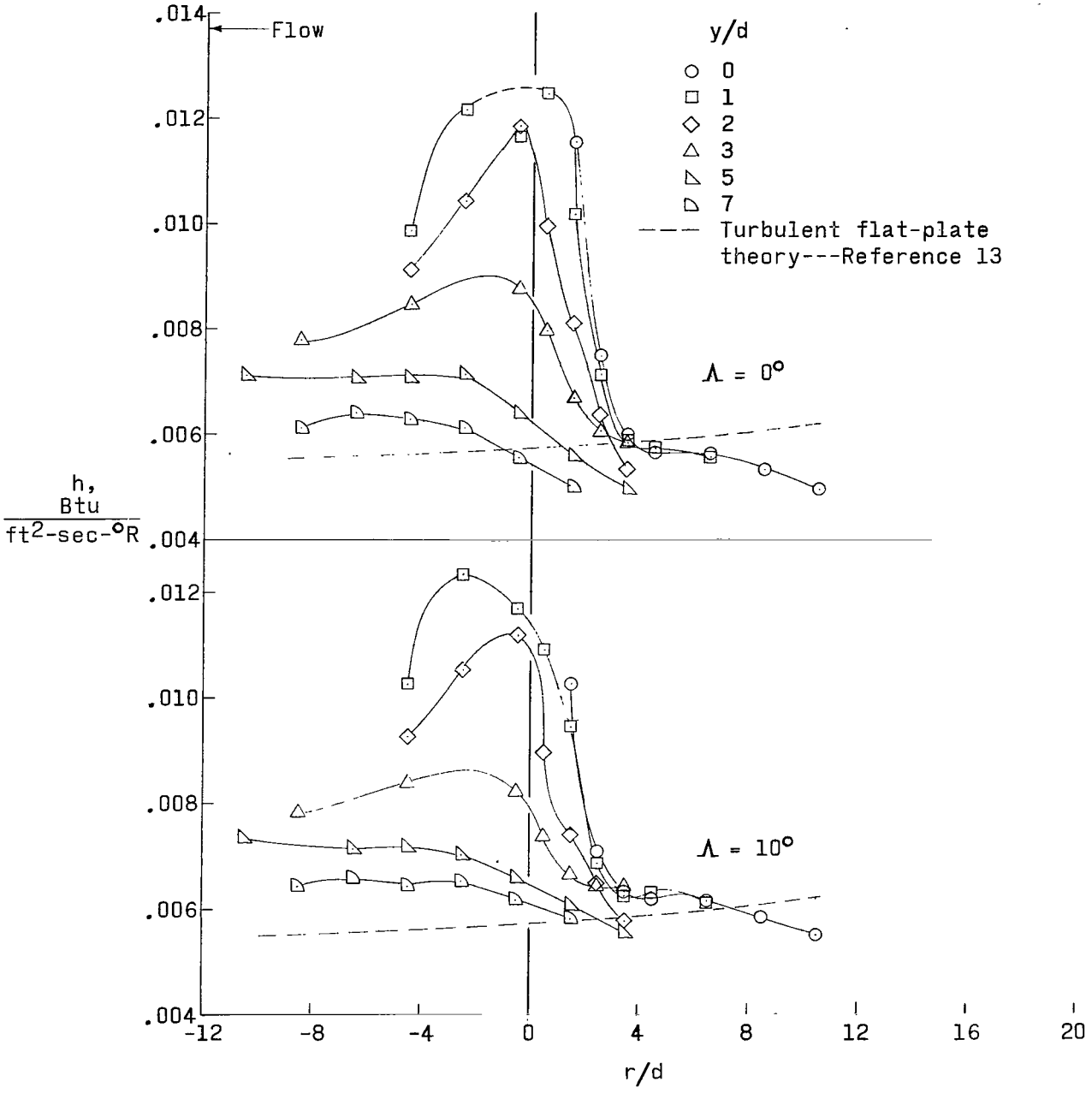

Figure 15.- Heating distribution on flat plate in vicinity of variable-sweep fin for range of sweep from 0° to 69°. M = 3.51; R ≈ 4.2 × 10^6; δ = 0.155 inch.

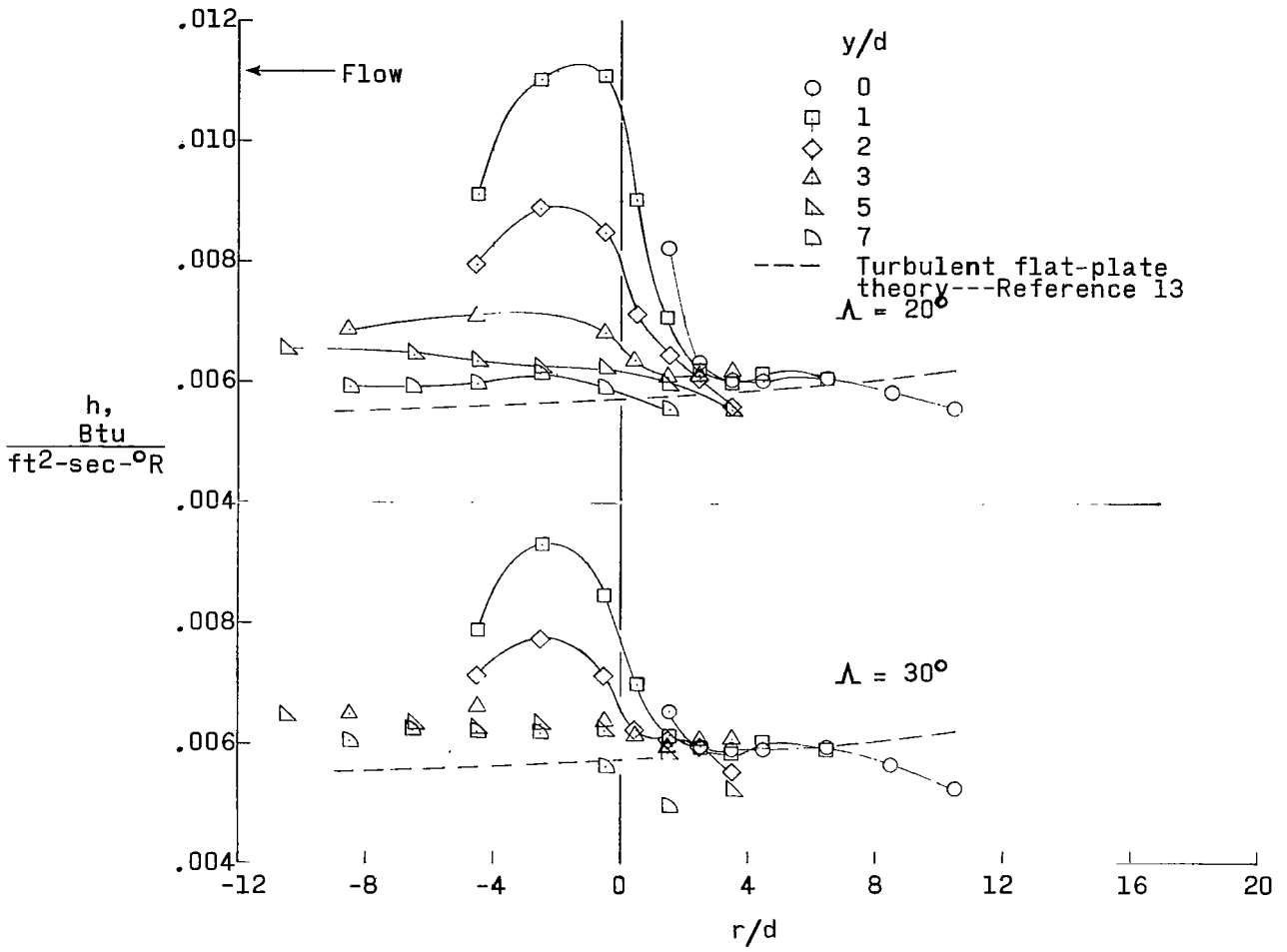

Figure 15.- Continued.

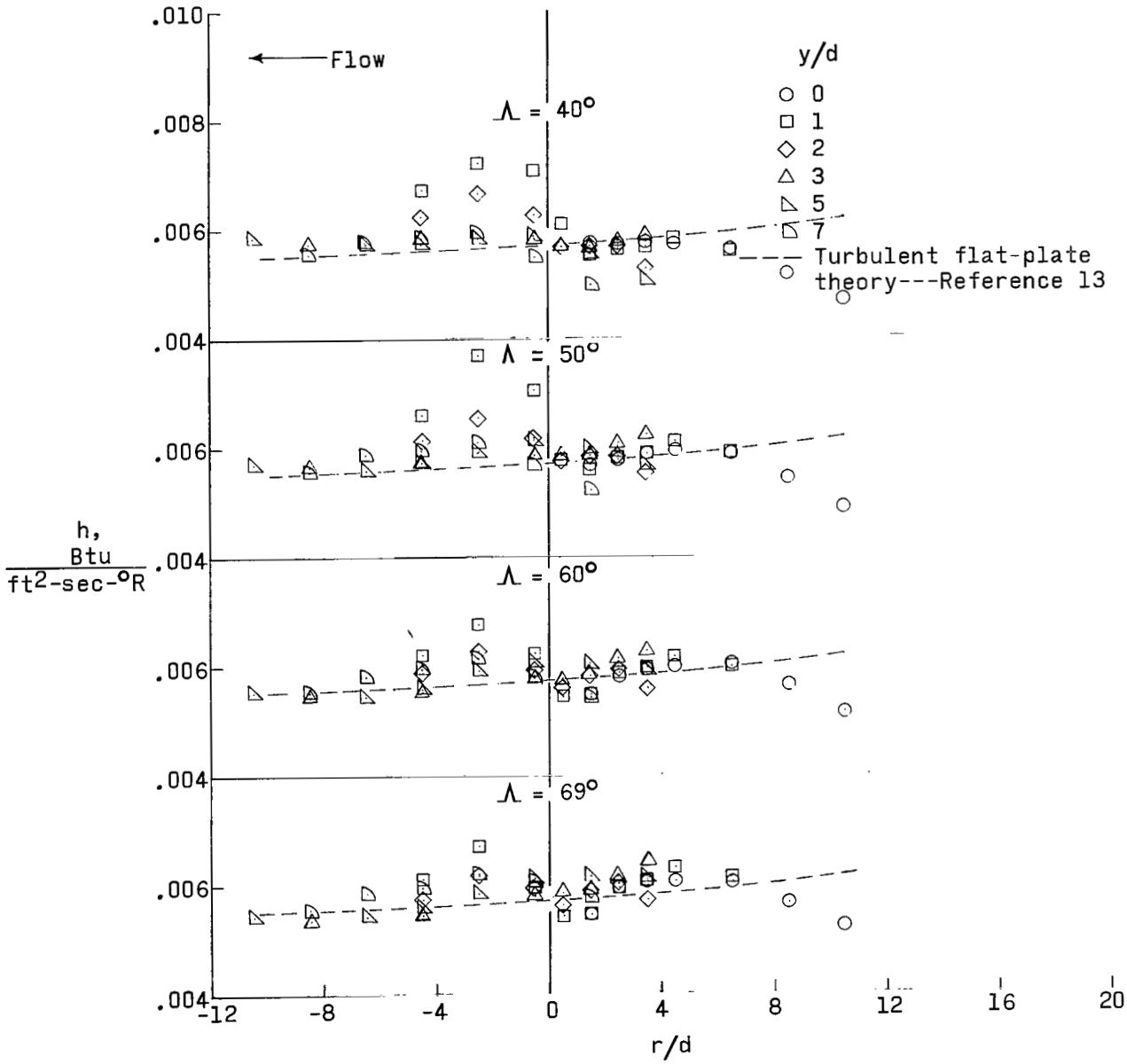

Figure 15.- Concluded.

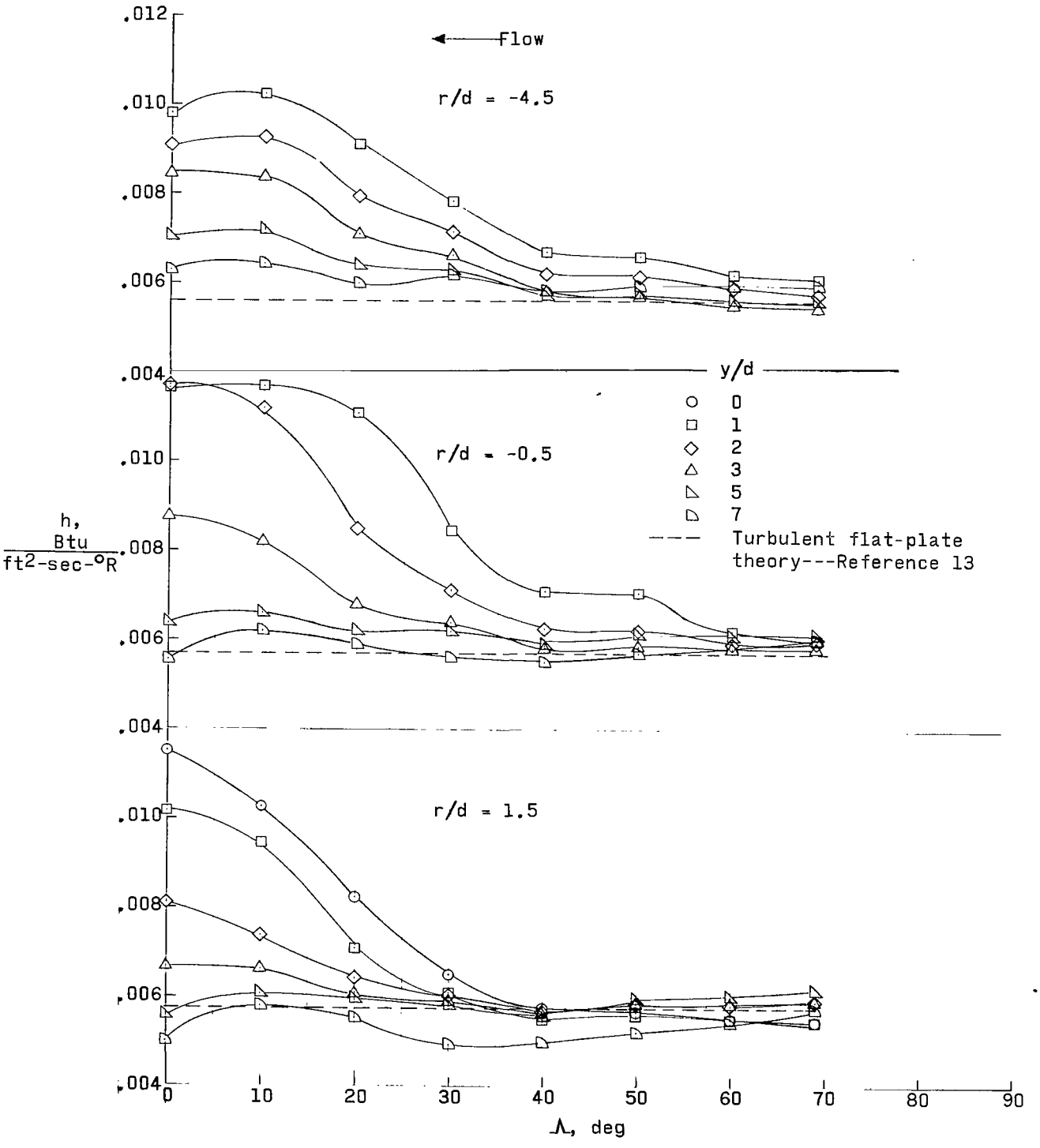

Figure 16.- Variation of heating rates with sweep angle for various values of y/d at three axial stations. M = 3.51; R ≈ 4.2×10^6; δ = 0.155 inch.

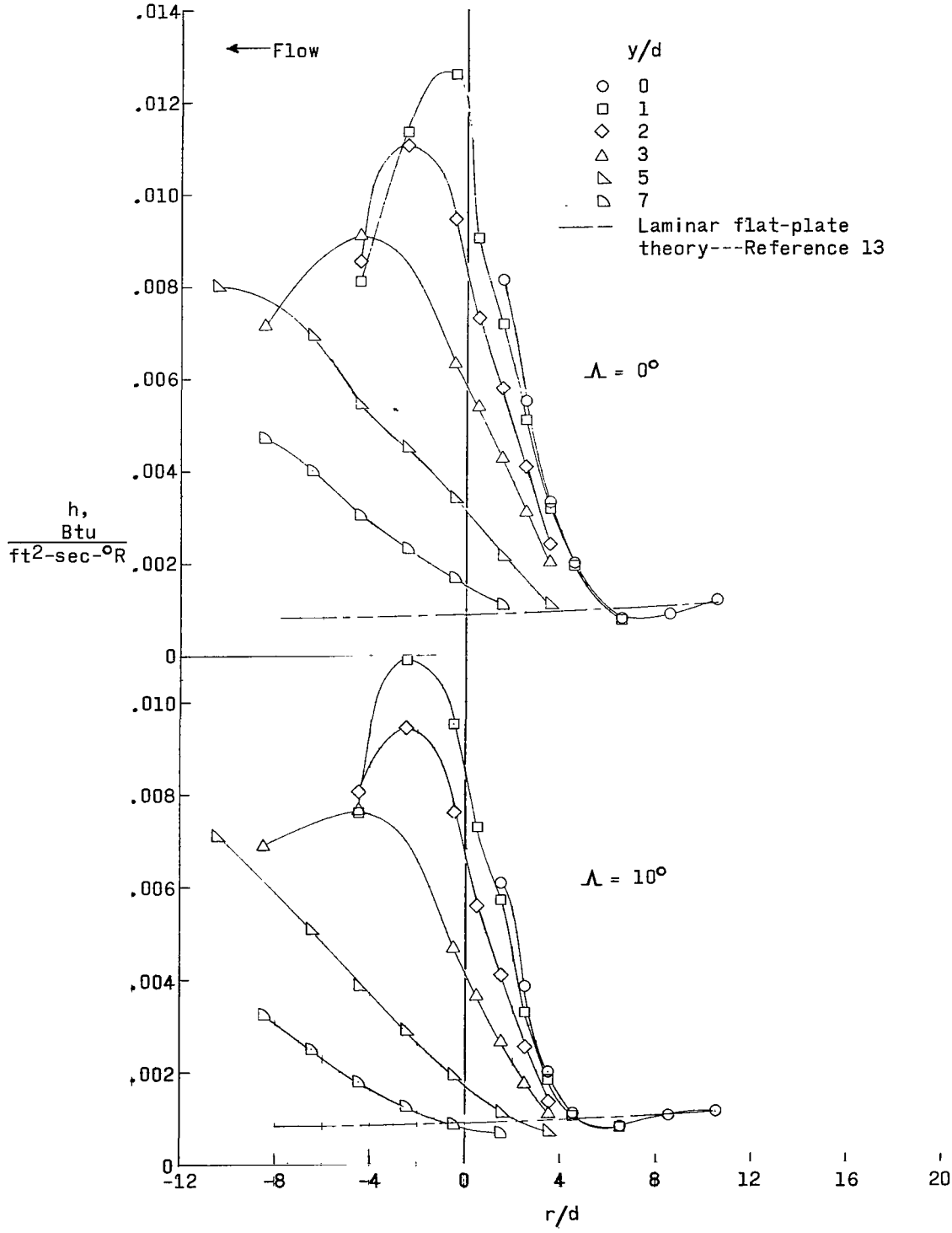

Figure 17.- Heating distribution on flat plate in vicinity of variable-sweep fin for range of sweep from 0° to 69°. M = 3.51; R ≈ 2.5×10^6.

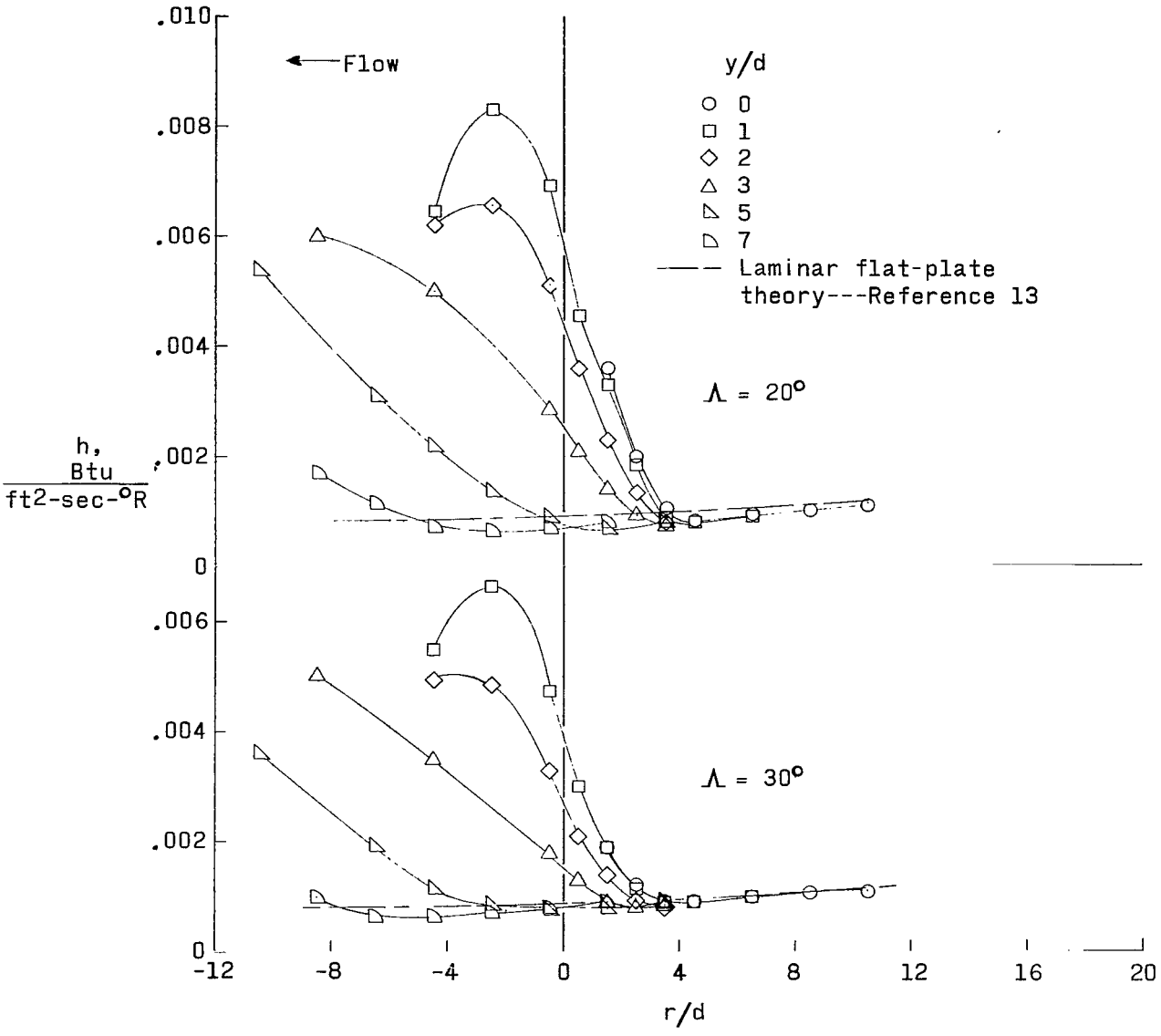

Figure 17.- Continued.

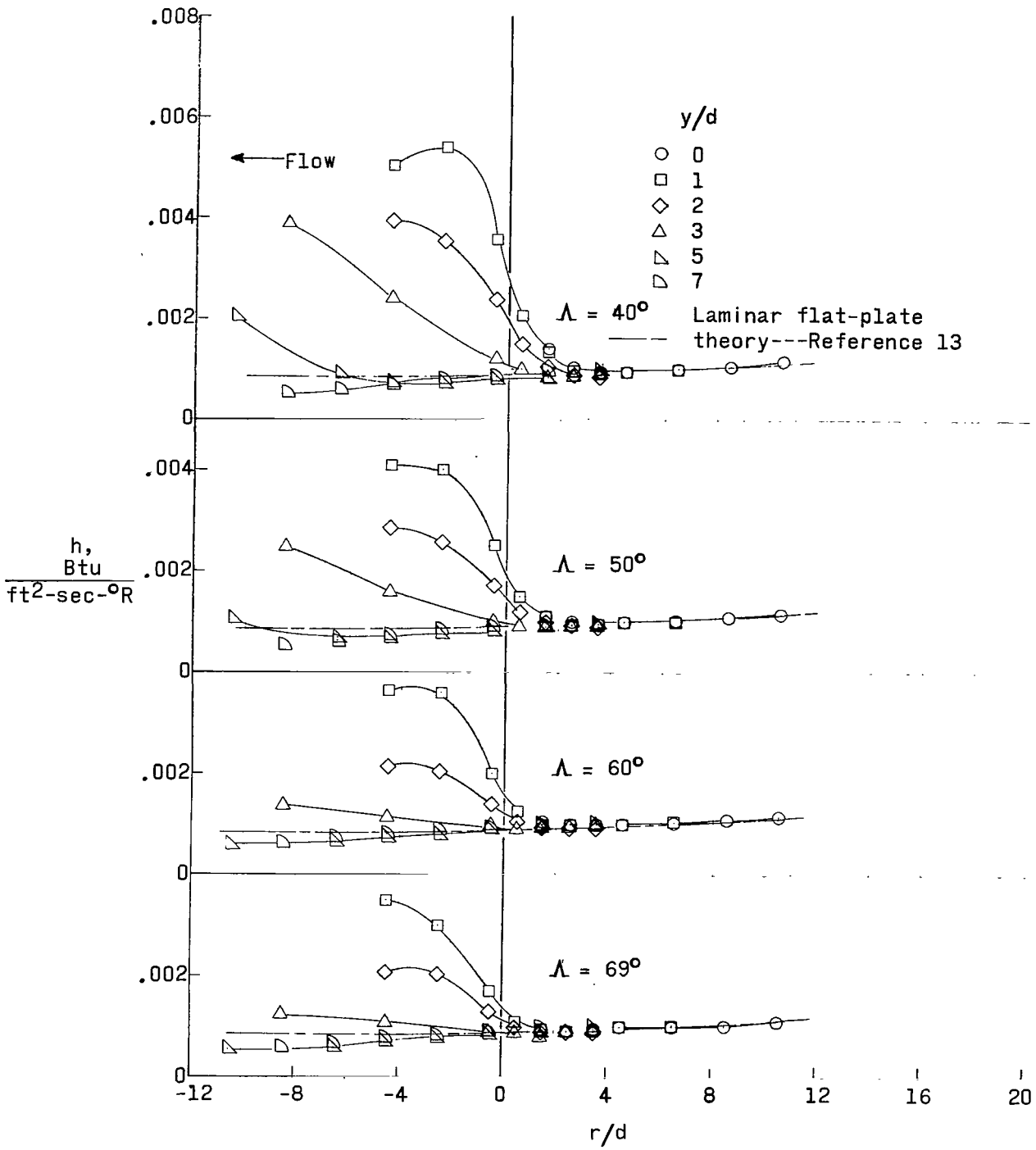

Figure 17.- Concluded.

NASA-Langley, 1964 L-3594

2 17 85

"The aeronautical and space activities of the United States shall be conducted so as to contribute . . . to the expansion of human knowledge of phenomena in the atmosphere and space. The Administration shall provide for the widest practicable and appropriate dissemination of information concerning its activities and the results thereof."

—NATIONAL AERONAUTICS AND SPACE ACT OF 1958

NASA SCIENTIFIC AND TECHNICAL PUBLICATIONS

TECHNICAL REPORTS: Scientific and technical information considered important, complete, and a lasting contribution to existing knowledge.

TECHNICAL NOTES: Information less broad in scope but nevertheless of importance as a contribution to existing knowledge.

TECHNICAL MEMORANDUMS: Information receiving limited distribution because of preliminary data, security classification, or other reasons.

CONTRACTOR REPORTS: Technical information generated in connection with a NASA contract or grant and released under NASA auspices.

TECHNICAL TRANSLATIONS: Information published in a foreign language considered to merit NASA distribution in English.

TECHNICAL REPRINTS: Information derived from NASA activities and initially published in the form of journal articles.

SPECIAL PUBLICATIONS: Information derived from or of value to NASA activities but not necessarily reporting the results of individual NASA-programmed scientific efforts. Publications include conference proceedings, monographs, data compilations, handbooks, sourcebooks, and special bibliographies.

Details on the availability of these publications may be obtained from:

SCIENTIFIC AND TECHNICAL INFORMATION DIVISION

NATIONAL AERONAUTICS AND SPACE ADMINISTRATION

Washington, D.C. 20546